

The catalogue of radial velocity variable hot subluminous stars from the MUCHFUSS project

S. Geier¹, T. Kupfer², U. Heber³, V. Schaffenroth^{3,4}, B. N. Barlow⁵, R. H. Østensen⁶, S. J. O’Toole⁷, E. Ziegerer³, C. Heuser³, P. F. L. Maxted⁸, B. T. Gänsicke⁹, T. R. Marsh⁹, R. Napiwotzki¹⁰, P. Brünner³, M. Schindewolf³, and F. Niederhofer¹

¹ European Southern Observatory, Karl-Schwarzschild-Str. 2, 85748 Garching, Germany

² Department of Astrophysics/IMAPP, Radboud University Nijmegen, P.O. Box 9010, 6500 GL Nijmegen, The Netherlands

³ Dr. Karl Remeis-Observatory & ECAP, Astronomical Institute, Friedrich-Alexander University Erlangen-Nuremberg, Sternwartstr. 7, D 96049 Bamberg, Germany

⁴ Institute for Astro- and Particle Physics, University of Innsbruck, Technikerstr. 25/8, 6020 Innsbruck, Austria

⁵ Department of Physics, High Point University, 833 Montlieu Avenue, High Point, NC 27268, USA

⁶ Institute of Astronomy, KU Leuven, Celestijnenlaan 200D, B-3001 Heverlee, Belgium

⁷ Australian Astronomical Observatory, PO Box 915, North Ryde NSW 1670, Australia

⁸ Astrophysics Group, Keele University, Staffordshire, ST5 5BG, UK

⁹ Department of Physics, University of Warwick, Coventry CV4 7AL, UK

¹⁰ Centre of Astrophysics Research, University of Hertfordshire, College Lane, Hatfield AL10 9AB, UK

Received Accepted

ABSTRACT

The project Massive Unseen Companions to Hot Faint Underluminous Stars from SDSS (MUCHFUSS) aims to find sdBs with compact companions like massive white dwarfs, neutron stars or black holes. Here we provide classifications, atmospheric parameters and a complete radial velocity (RV) catalogue containing 1914 single measurements for an sample of 177 hot subluminous stars discovered based on SDSS DR7. 110 stars show significant RV variability, while 67 qualify as candidates. We constrain the fraction of close massive compact companions of hydrogen-rich hot subdwarfs in our sample to be smaller than $\sim 1.3\%$, which is already close to the theoretical predictions. However, the sample might still contain such binaries with longer periods exceeding ~ 8 d. We detect a mismatch between the ΔRV_{\max} -distribution of the sdB and the more evolved sdOB and sdO stars, which challenges our understanding of their evolutionary connection. Furthermore, irregular RV variations of unknown origin with amplitudes of up to $\sim 180 \text{ km s}^{-1}$ on timescales of years, days and even hours have been detected in some He-sdO stars. They might be connected to irregular photometric variations in some cases.

Key words. binaries: spectroscopic – stars: subdwarfs – stars: horizontal branch – stars: atmospheres

1. Introduction

Hot subdwarf stars (sdO/Bs) show spectral features similar to hot main sequence stars, but are much less luminous and therefore more compact. Depending on their spectral appearance, hot subdwarf stars can be divided into subclasses (Moehler et al. 1990; see Drilling et al. 2013 for a more detailed classification scheme). While the observational classification seems straightforward, the formation and evolution of those objects is still unclear.

In the Hertzsprung-Russell diagram most hot subdwarf stars are situated at the blueward extension of the Horizontal Branch (HB), the so called Extreme or Extended Horizontal Branch (EHB, Heber et al. 1986). The most common class of hot subdwarfs, the sdB stars, are located on the EHB and are therefore considered to be core-helium burning stars. They have very thin hydrogen dominated atmospheres ($M_{\text{env}}/M_{\text{sdB}} \approx 10^{-3}$, $n_{\text{He}}/n_{\text{H}} \leq 0.01$), their effective temperatures (T_{eff}) range from 20 000 K to 40 000 K and their surface gravities ($\log g$) are one to two orders

of magnitude higher than those of main sequence stars of the same spectral type (usually between $\log g = 5.0$ and 6.0).

SdB stars are likely formed from stars that almost entirely lose their hydrogen envelopes after climbing up the red giant branch (RGB). The outer layer of hydrogen that remains does not have enough mass to sustain a hydrogen-burning shell, as is the case for cooler HB stars. Therefore the star can not evolve in the canonical way and ascend the Asymptotic Giant Branch (AGB). Instead the star remains on the EHB until core-helium burning stops, and after a short time of shell-helium burning eventually reaches the white dwarf (WD) cooling tracks. According to evolutionary calculations the average lifetime on the EHB is of the order of 10^8 yr (e.g. Dorman et al. 1993). In this canonical scenario the hotter ($T_{\text{eff}} = 40\,000 - 80\,000$ K) and much less numerous hydrogen rich sdOs can be explained as rather short-lived shell-helium burning stars evolving away from the EHB.

Systematic surveys for radial velocity (RV) variations revealed that a large fraction of the sdB stars (40 – 70 %) are members of close binaries with orbital periods ranging from ≈ 0.05 d to ≈ 30 d (Maxted et al. 2001; Morales-Rueda et al. 2003; Copperwheat et al. 2011). Most of the known companions of sdBs in radial velocity variable close binary systems are white

Send offprint requests to: S. Geier,
e-mail: sgeier@eso.org

Table 1. Telescopes and instrumental setups

Telescope	Instrument	R	$\Delta\lambda$ [Å]
Sloan	SDSS	1800	3800 – 9200
ESO-VLT	FORS1	1800	3730 – 5200
WHT	ISIS	4000	3440 – 5270
CAHA-3.5m	TWIN	4000	3460 – 5630
ESO-NTT	EFOSC2	2200	4450 – 5110
SOAR	Goodman	2500	3500 – 6160 ^a
	Goodman	7700	3700 – 4400
Gemini	GMOS-N/S	1200	3770 – 4240
INT	IDS	1400	3000 – 6800
	IDS	4000	3930 – 5100 ^b
SAAO-1.9m	Grating	4600	4170 – 5030

Notes. ^(a) Used until 2011. ^(b) Additional data taken in March 2003 and April 2004.

dwarfs or late type main sequence stars, but substellar companions like brown dwarfs have been found as well (see Kupfer et al. 2015 and references therein). Those systems were most likely formed after a common envelope (CE) and spiral-in phase, which also provides an explanation for the required mass-loss on the RGB. However, apparently single sdBs and wide binary systems (Vos et al. 2012, 2013; Barlow et al. 2013) exist as well. In those cases, it is less straightforward to explain the formation of the sdBs (see Geier 2013 for a review).

Hot subdwarf binaries with massive WD companions are good candidates for SN Ia progenitors. Due to gravitational wave radiation the orbit will shrink further and mass transfer from the sdB onto the WD will start once the sdB fills its Roche lobe. The Chandrasekhar limit might be reached either through He accretion on the WD (e.g. Yoon & Langer 2004 and references therein) or a subsequent merger of the system (Tutukov et al. 1981; Webbink 1984). Two sdBs with massive WD companions have been identified to be good candidates for being SN Ia progenitors (Maxted et al. 2000a; Geier et al. 2007; Vennes et al. 2012; Geier et al. 2013b). Neutron star (NS) or even black hole (BH) companions are predicted by theory as well (Podsiadlowski et al. 2002; Pfahl et al. 2003). In this scenario two phases of unstable mass transfer are needed and the NS or the BH is formed in a supernova explosion. Nelemans (2010) showed that about 1% of the short period sdBs should have NS companions whereas about 0.1% should have BH companions. In an independent study Yungelson et al. (2005) predicted the number of systems with NS companions to be about 0.8%. However, no NS/BH companion to an sdB has yet been detected unambiguously whereas a few candidates have been identified (Geier et al. 2010b). Most recently, Kaplan et al. (2013) discovered the close companion to the pulsar PSR J1816+4510 to be a He-WD progenitor with atmospheric parameters close to an sdB star ($T_{\text{eff}} = 16\,000$ K, $\log g = 4.9$).

The formation of the helium-rich classes of He-sdO/Bs is even more puzzling. Most (but not all) He-sdOs are concentrated in a very small region in the $T_{\text{eff}}\text{-}\log g$ plane, slightly blueward of the EHB at $T_{\text{eff}} = 40\,000 - 80\,000$ K and $\log g = 5.60 - 6.10$ (Ströer et al. 2007; Nemeth et al. 2012). The He-sdBs are scattered above the EHB. The late hot flasher scenario provides a possible channel to form these objects (Lanz et al. 2004; Miller Bertolami et al. 2008). After ejecting most of its envelope at the tip of the RGB, the stellar remnant evolves directly towards the WD cooling tracks and experiences a late core helium flash

there. Helium and other elements like carbon or nitrogen are mixed into the atmosphere and the star ends up close to the helium main sequence. Depending on the depth of the mixing, stars with more or less helium in the atmospheres and different atmospheric parameters can be formed in this way. Most recently, Latour et al. (2014) found a correlation between the carbon and helium abundances of the He-sdOB stars in the globular cluster ω Cen, which is predicted by late hot flasher models. Hirsch (2009) discovered a similar correlation for field helium-rich hot subdwarf (see also Heber & Hirsch 2010). Similar to the formation scenarios for sdB stars, the late hot flasher channel requires extreme mass-loss on the RGB probably triggered by binary interactions. However, the population of He-sdOs observed so far seems to consist mostly of single stars. Only one RV-variable He-sdO has been reported in the SPY sample, which corresponds to a fraction of only 3% (Napiwotzki 2008). However, higher fractions have been reported for the He-sdO populations in the PG sample (Green et al. 2008).

An alternative way of forming single hot subdwarfs is the merger of two helium white dwarfs in a close binary (Webbink 1984; Iben & Tutukov 1984). Loss of angular momentum through the emission of gravitational radiation will cause the system to shrink. Given the initial separation is small enough, the two white dwarfs eventually merge and if the mass of the merger is high enough, core-helium burning is ignited and a hot subdwarf is formed. Due to the strong mixing during the merger process, the atmospheres of the merger products are expected to be helium-rich (Zhang & Jeffery 2012).

Some hot subluminoous stars are not connected to EHB-evolution at all. Objects with spectra and atmospheric parameters similar to normal sdBs are known, which are situated below the EHB (e.g. Heber et al. 2003; Silvotti et al. 2012). These objects are considered to be direct progenitors of helium white dwarfs, which descend from the red giant branch. For these low-mass post-RGB objects, which cross the EHB, evolutionary tracks indicate masses of about $0.20 - 0.33 M_{\odot}$ (Driebe et al. 1998). In order to form such objects, the mass loss on the RGB has to be more extreme than in the case of EHB stars. Objects down to even lower masses are known as extremely low-mass (ELM) WDs, which are members of close binary systems (e.g. Brown et al. 2012). More massive He-stars, like the so-called low-gravity or luminous He-sdOs (Jeffery et al. 2008) also belong to the class of hot subdwarfs and are situated between the EHB and the main sequence.

2. The MUCHFUSS project

The project Massive Unseen Companions to Hot Faint Underluminoous Stars from SDSS (MUCHFUSS) aims to find hot subdwarf stars with massive compact companions like massive white dwarfs ($> 1.0 M_{\odot}$), neutron stars or stellar mass black holes. Hot subdwarf stars were selected from the Sloan Digital Sky Survey by colour and visual inspection of the spectra. Hot subdwarf stars with high radial velocity variations were selected as candidates for follow-up spectroscopy to derive the radial velocity curves and the binary mass functions of the systems.

Geier et al. (2011a) discussed the target selection and the follow-up strategy. Detailed analyses of sdB binaries discovered in the course of this project are given in Geier et al. (2011b) and Kupfer et al. (2015). Three eclipsing systems have been discovered, two of them being the first sdBs with brown dwarf companions (Geier et al. 2011c; Schafferoth et al. 2014). One system turned out to be the first sdB hybrid pulsator showing a reflection effect (Østensen et al. 2013). The photometric follow-

up campaign of the MUCHFUSS project will be described in detail in Schaffenroth et al. (in prep). During dedicated spectroscopic MUCHFUSS follow-up runs bright sdB binary candidates were observed in a supplementary programme (Geier et al. 2013b, 2014a). Hot subdwarfs with a high but constant radial velocity were studied in the Hyper-MUCHFUSS project (Tillich et al. 2011).

Here we present classifications, radial velocities and atmospheric parameters of the close binary candidates discovered in the MUCHFUSS project so far. In Sect. 3 we describe the observations, target selection, classification and quantitative spectral analysis of our sample as well as the radial velocity catalogue. In Sect. 4 the different populations of RV variable hot subluminous stars are presented and discussed. A summary is then given in Sect. 5.

3. Target selection, observations, spectroscopic analysis

3.1. Observations and sample selection

While the target selection presented in Geier et al. (2011a) includes SDSS up to Data Release 6 only, we have now applied the same selection criteria to Data Release 7 (Abazajian et al. 2009). Hot subdwarf candidates were selected by applying a colour cut to SDSS photometry. All point source spectra within the colours $u - g < 0.4$ and $g - r < 0.1$ were selected and downloaded from the SDSS Data Archive Server¹. By visual inspection we selected and classified $\approx 10\,000$ hot stars. Most objects much fainter than $g = 19$ mag have been excluded because of insufficient quality. The sample contains 1369 hot subdwarfs, consistent with the preliminary number of hot subdwarfs (1409) found by Kleinman et al. (2010) in SDSS-DR7.

The SDSS spectra are co-added from at least three individual integrations with typical exposure times of 15 min taken consecutively. We have obtained those individual spectra for stars brighter than $g = 18.5$ mag. In addition, second epoch medium resolution spectroscopy was obtained from SDSS as well as our own observations, using ESO-VLT/FORS1, WHT/ISIS, CAHA-3.5m/TWIN and ESO-NTT/EFOSC2 (see Table 1, Geier et al. 2011a). Typical exposure times ranged from 10 min to 20 min. The S/N of the individual spectra ranges from about 15 to about 100.

The radial velocities were measured by fitting a set of mathematical functions (Gaussians, Lorentzians and polynomials) to the spectral lines using the FITSB2 routine (Napiwotzki et al. 2004). Three functions are used to match the continuum, the line and the line core, respectively and mimic the typical Voigt profile of spectral lines. The profiles are fitted to all suitable lines simultaneously using χ^2 -minimization and the RV shift with respect to the rest wavelengths with the associated 1σ error is measured. For the hydrogen-rich stars the Balmer and helium lines of sufficient strength have been used. For the helium-rich stars we used appropriate lines of neutral and single ionized helium. Since some of those stars still have significant hydrogen contamination we avoided the helium lines from the Pickering series, because they can be blended by the weaker hydrogen Balmer lines. Each single fit has been inspected visually and outliers caused by cosmic rays and other artifacts have been excluded. Heliocentric corrections have been applied to the RVs and mid-JDs derived for the follow-up spectra, while the SDSS spectra available in the archive are already corrected.

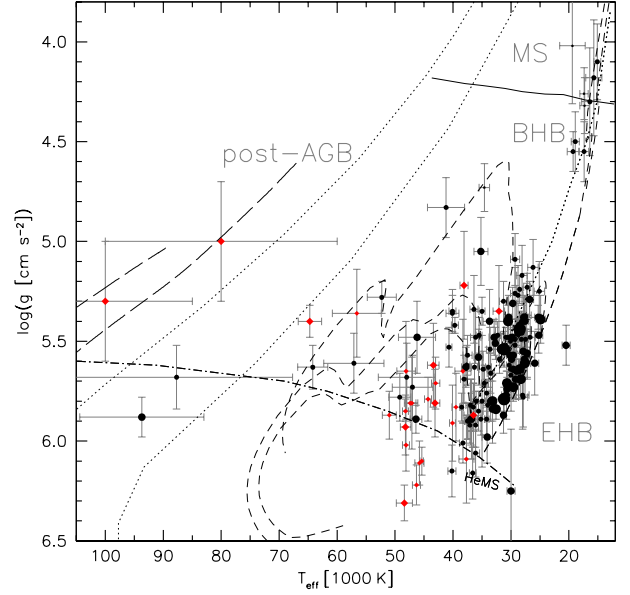


Fig. 1. $T_{\text{eff}} - \log g$ diagram of the full sample of hot, subluminous, RV-variable stars. The size of the symbols scales with ΔRV_{max} . The black circles mark stars with hydrogen dominated atmospheres ($\log y < 0$), while the red diamonds mark stars with helium dominated atmospheres. The helium main sequence (HeMS) and the HB band are superimposed with HB evolutionary tracks (dashed lines) for subsolar metallicity ($\log z = -1.48$) from Dorman et al. (1993). The three tracks in the high temperature range correspond to helium core masses of 0.488 , 0.490 and $0.495 M_{\odot}$ (from bottom-left to top-right). Those tracks mark the EHB evolution, since the stars do not reascend the giant branch in the helium shell-burning phase. The two tracks in the upper right correspond to core masses of 0.53 and $0.54 M_{\odot}$. BHB stars following those tracks are expected to experience a second giant phase. The solid line marks the relevant part of the zero-age main sequence for solar metallicity taken from Schaller et al. (1992). The two dotted lines are post-AGB tracks for hydrogen-rich stars with masses of 0.546 (lower line) and $0.565 M_{\odot}$ (upper line) taken from Schönberner (1983). The two long-dashed lines are post-AGB tracks for helium-rich stars with masses of 0.53 (lower line) and $0.609 M_{\odot}$ (upper line) taken from Althaus et al. (2009).

The average 1σ RV error of all the measurements in the catalogue is $\sim 15 \text{ km s}^{-1}$, which is consistent with independent checks of the SDSS wavelength stability using SDSS observations of F-stars ($< 14.5 \text{ km s}^{-1}$, Rebassa-Mansergas et al. 2007). To correct for systematic shifts between different instruments we observed RV standards in our follow-up runs. The RMS scatter around the orbital fits of the solved binaries in our sample is also consistent with the formal uncertainties (for details, see Geier et al. 2011b; Kupfer et al. 2015). We selected all objects with maximum RV shifts discrepant at the formal 1σ -level and found 196 candidates for RV variability.

3.2. Visual classification

The basic classification of the hot subdwarf sample was done by visual inspection based on existence, width, and depth of

¹ das.sdss.org

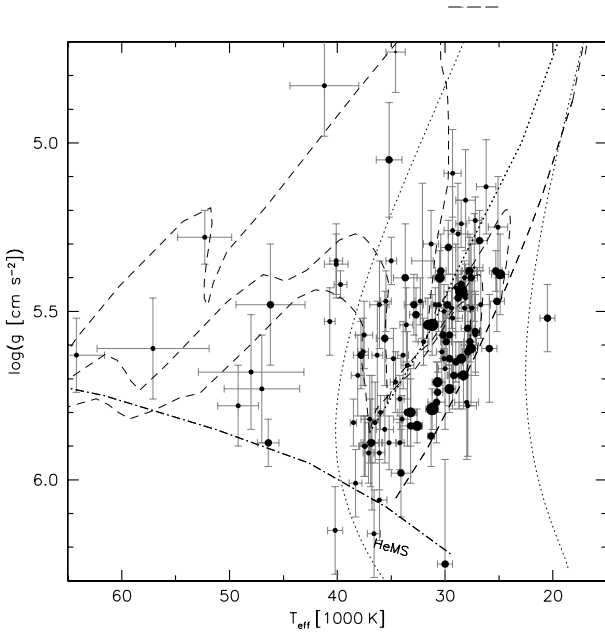


Fig. 2. $T_{\text{eff}} - \log g$ diagram of RV variable hydrogen-rich sdB and sdOB stars (see Fig. 1). The size of the symbols scales with ΔRV_{max} . The helium main sequence (HeMS) and the HB band are superimposed with HB evolutionary tracks (dashed lines) for subsolar metallicity ($\log z = -1.48$) from Dorman et al. (1993). The three tracks correspond to helium core masses of 0.488, 0.490 and 0.495 M_{\odot} (from bottom-left to top-right). The two dotted lines mark post-RGB tracks (Driebe et al. 1998) for core masses of 0.234 (left) and 0.259 M_{\odot} (right).

helium and hydrogen absorption lines as well as the flux distribution between 4000 and 6000 Å. Hot subdwarf B stars show strong and broad Balmer and weak (or no) He I lines. SdOB stars show strong and broad Balmer lines as well as weak lines from He I and He II, while sdO stars only display weak He II lines besides the Balmer lines. He-sdBs are dominated by strong He I and sometimes weaker He II lines. Hydrogen absorption lines are shallow or not present at all. He-sdOs show strong He II and sometimes weak He I lines. Balmer lines are not present or heavily blended by the strong He II lines of the Pickering series. A flux excess in the red compared to a reference spectrum as well as the presence of spectral features such as the Mg I triplet at 5170 Å or the Ca II triplet at 8650 Å were taken as indications of a late-type companion.

From the total number of 1369 hot subdwarfs, 983 belong to the class of single-lined sdBs and sdOBs. Features indicative of a cool companion were found for 98 of the sdBs and sdOBs. Nine sdOs show spectral features of cool companions, while 262 sdOs, most of which show helium enrichment, are single-lined.

Comparing the results from the visual classification with the more detailed quantitative spectral analysis for the RV variable subsample presented here (see Sect. 4), we conclude that our visual classification should be accurate to about 90%. A catalogue with classifications and atmospheric parameters of the full SDSS sample including more recent data releases is in preparation. Here we restrict ourselves to the RV-variable sample.

3.3. Atmospheric parameters and spectroscopic distances

To refine the visual classification and derive the atmospheric parameters a quantitative spectral analysis of the coadded SDSS spectra (or follow-up spectra of higher quality, if available) was performed for all RV variable stars in our sample with data of sufficient quality. The method is described in Geier et al. (2011b). We used appropriate model grids for the different classes of hot stars. The hydrogen-rich and helium-poor ($\log y = \log n(\text{He})/n(\text{H}) < -1.0$) stars with effective temperatures below 30 000 K were fitted using a grid of metal line blanketed LTE atmospheres with solar metallicity. Helium-poor stars with temperatures ranging from 30 000 K to 40 000 K were analysed using LTE models with enhanced metal line blanketing (O’Toole & Heber 2006). Metal-free NLTE models (Ströer et al. 2007) were used for hydrogen-rich stars with temperatures below 40 000 K showing moderate He-enrichment ($\log y = -1.0 - 0.0$) and for hydrogen-rich sdOs. Finally, the He-sdOs were analysed with NLTE models taking into account the line-blanketing caused by nitrogen and carbon (Hirsch & Heber 2009).

Spectroscopic distances to our stars have been calculated as described in Ramspeck et al. (2001) assuming the canonical mass of 0.47 M_{\odot} for the subdwarfs and appropriate masses for objects of other classes (0.5 M_{\odot} for blue horizontal branch star candidates and 3.5 M_{\odot} for runaway main-sequence B star candidates, Geier et al. 2015; 0.6 M_{\odot} for post-AGB stars, Reindl et al. 2015) using the formula given by Lupton² to convert SDSS- g and r magnitudes to Johnson V magnitudes. Interstellar reddening was neglected in these calculations.

3.4. Spectroscopic follow-up, criterion for variability and radial velocity catalogue

During our follow-up campaign we obtained medium resolution ($R = 1200 - 7700$), time-resolved spectroscopy using WHT/ISIS, CAHA3.5m/TWIN, ESO-NTT/EFOSC2, SOAR/Goodman, Gemini/GMOS, INT/IDS and the grating spectrograph at the 1.9m telescope at SAAO (see Table 1, Geier et al. 2011b; Kupfer et al. 2015) and measured the RVs as described above.

To estimate the fraction of false detections produced by random fluctuations and calculate the significance of the measured RV variations we apply the method outlined in Maxted et al. (2001). For each star we calculate the inverse-variance weighted mean velocity from all measured epochs. Assuming this mean velocity to be constant, we calculate the χ^2 . Comparing this value with the χ^2 -distribution for the appropriate number of degrees of freedom we calculate the probability p of obtaining the observed value of χ^2 or higher from random fluctuations around a constant value. The maximum RV shifts (ΔRV_{max}), the average 1σ uncertainties of the two corresponding measurements, the timespan between those two epochs and the logarithm of the false-detection probability $\log p$ are given in Tables 3-5.

We consider the detection of RV variability to be significant, if the false-detection probability p is smaller than 0.01% ($\log p < -4.0$). The fraction of such significant detections in our initial sample of 196 is 56% (110 objects). Objects with false-detection probabilities between 0.01% and 5% ($\log p = -4.0$ to $\log p = -1.3$) are regarded as candidates for RV variability and constitute 34% of the initial sample (67 objects). About 10% ($\log p > -1.3$, 19 objects) are regarded as non-detections (the parameters of those stars can be found in Table A.1). Removing

² <http://www.sdss.org/dr6/algorithms/sdssUBVRITransform.html>

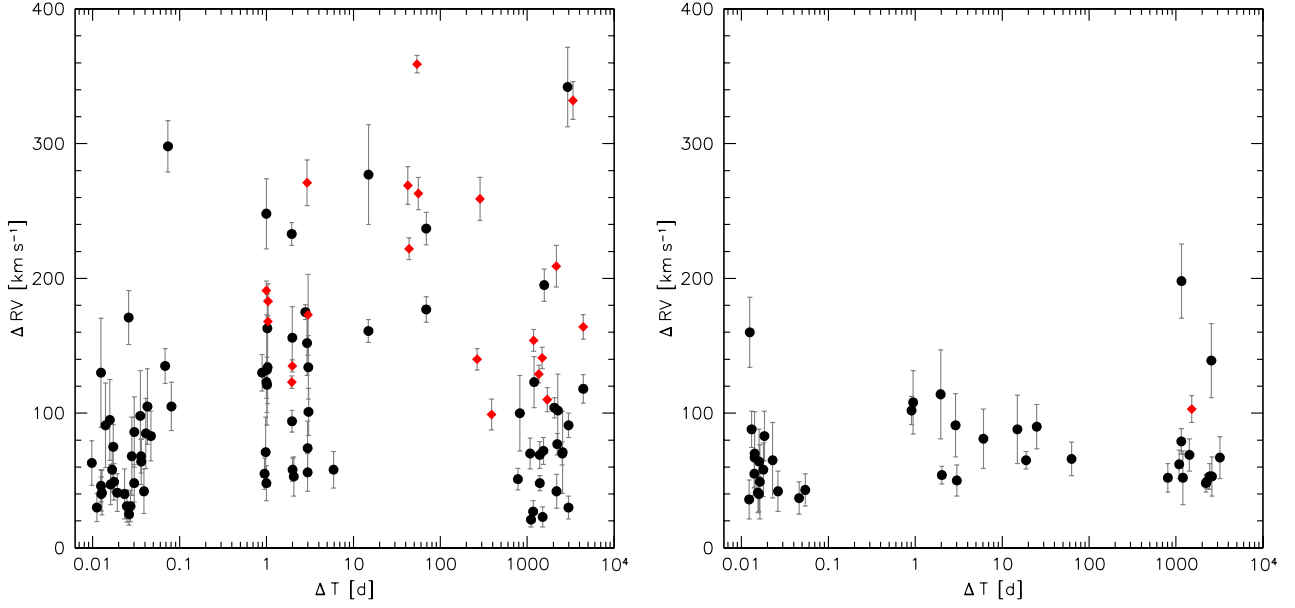


Fig. 3. *Left panel:* Highest radial velocity shift between individual spectra plotted against time difference between the corresponding observing epochs. The filled red diamonds mark sdB binaries with known orbital parameters (Kupfer et al. 2015), while the filled black circles mark the rest of the hydrogen-rich sdB sample of RV variable stars. *Right panel:* The same plot for the hydrogen-rich sdOB and sdO sample of RV variable stars.

Table 2. Sample statistics

Class	RV variable	RV variable candidates	non-detections
H-rich sdO/B	89	50	13
He-rich sdO/B	14	11	4
Others	7	6	2
Total	110	67	19

those non-detections we end up with a sample of 177 stars, which show RV variability with probabilities between 95% and 99.9% (see Table 2). Orbital solutions were already derived for 22 close binary sdB systems (see Kupfer et al. 2015 and references therein).

The catalogue contains 1914 epochs (mid-HJD), associated radial velocities and 1σ -RV-uncertainties of the RV variable stars as well as information about the instruments used to obtain the spectra. It can be accessed online from the VizieR database operated by CDS.

4. Radial velocity variable populations of hot subluminoous stars

Since our sample has been preselected in the way outlined above it is not straightforward to derive the true fractions of RV variable stars for each class of hot subdwarfs. Most stars in our sample have been selected based on RV variations between the individual SDSS spectra, which have usually been taken within just 45 min. Only binaries with sufficiently short orbital periods and high RV amplitudes show significant variations on such

short timescales, while binaries with smaller RV amplitudes and longer periods remain undetected.

Fig. 1 shows the $T_{\text{eff}} - \log g$ -diagram of the RV variable sample. Most of the stars are indeed associated with the EHB and therefore most likely core or shell-helium burning hot subdwarfs. Four objects have higher temperatures and are more likely hydrogen and helium-rich post-AGB objects. Nine stars have temperatures below 20 000 K and most of them are likely associated with the blue horizontal branch (see Table 5). The B-type binary candidates are discussed separately in Geier et al. (2015), the hot post-AGB stars in Reindl et al. (2015).

Although only the orbits of 22 binaries from our sample have been solved, the distribution of ΔRV_{max} can be used as a diagnostic tool as well. The width of this distribution scales with the width of the companion mass distribution as well as the distribution of orbital periods.

4.1. Hydrogen-rich hot subdwarf stars and their evolutionary connection

The most common class of RV variable objects in our sample are sdB, sdOB and sdO stars with hydrogen-dominated atmospheres (see Table 3). Fig. 2 shows the $T_{\text{eff}} - \log g$ -diagram of this subsample. As expected, most objects are concentrated on the EHB and some objects follow the tracks of more evolved shell-helium burning stars. This distribution is consistent with other studies (e.g. Nemeth et al. 2012). However, it is not clear whether all objects situated above the EHB are really shell-helium burning stars and might constitute a certain fraction of stars in this region of the $T_{\text{eff}} - \log g$ -diagram.

The detected RV-variability in those objects is very likely caused by binary motion. Up to now the orbital parameters of

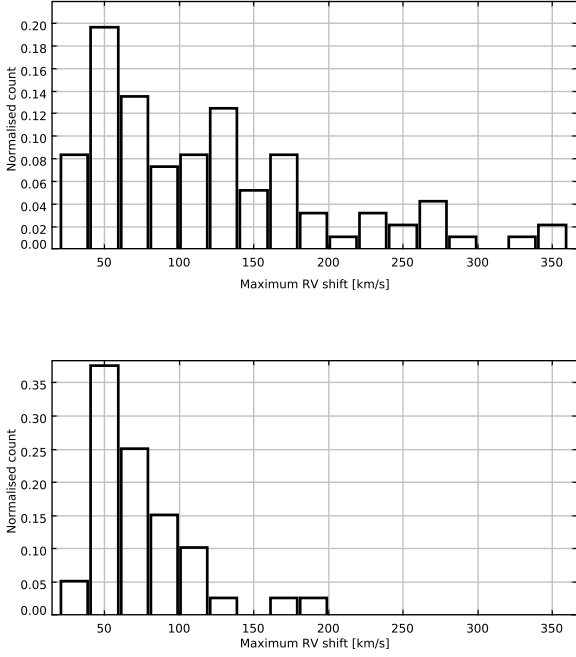


Fig. 4. ΔRV_{\max} distribution of RV-variable sdB stars (upper panel) as well as sdOB and sdO stars with hydrogen-rich atmospheres (lower panel).

142 close binaries have been measured. Most of the solved systems have hydrogen-rich sdB primaries, but this sample also contains 46 hydrogen-rich sdOB and sdO stars (see Kupfer et al. 2015 and references therein, but see also the discussion in Sect. 4.5). Another possible source of RV-variations are short-period p-mode pulsations. However, the fraction of pulsating hot subdwarf stars is quite small (about 5%) and the RV-variations are usually smaller than our detection limit. Even in the most extreme cases known, where those variations can reach amplitudes of $10 - 20 \text{ km s}^{-1}$ (e.g. O’Toole et al. 2005), we would most likely not resolve and detect them in our data, because our exposure times are usually longer than the typical periods (a few minutes) of those pulsations.

The additional information provided by the RV variability (Table 3, Fig. 3) allows us to probe the connection between objects on the EHB classified as sdBs (100 RV variable objects) with stars that are situated above the EHB classified as sdOB or sdO (40 RV-variable objects). While the internal structure and the atmospheric parameters of the hot subdwarf change with time, the orbital period and the companion mass are not predicted to change significantly within the lifetime of the sdB ($\sim 100 \text{ Myr}$). A significant shortening of the orbital period due to angular momentum lost by gravitational wave emission is only predicted for the most compact binaries with the most massive companions, which turned out to be quite rare (e.g. Geier et al. 2007, 2013b). Furthermore, the orbital evolution will always lead to shorter periods and therefore higher RV-amplitudes. If the sdBs on the EHB evolve to become hydrogen-rich sdOB and sdO stars, the ΔRV_{\max} -distribution should essentially remain the same.

Fig. 4 shows the ΔRV_{\max} -distribution of both subsamples. While the distribution below 100 km s^{-1} looks very similar as expected, the sdB sample shows a wider range of RV shifts (see

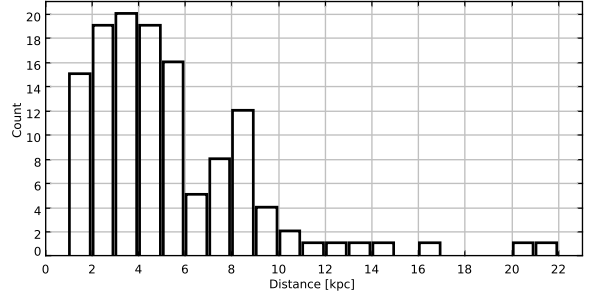


Fig. 5. Distribution of spectroscopic distances for the hydrogen-rich sdB, sdOB and sdO stars (see Table 3).

also Fig. 3). This can only be partly explained by the smaller size of the sdOB/sdO sample. There are also no significant differences in data quality and temporal sampling between the two different groups. Essentially the same hydrogen Balmer lines have been used to measure the RVs. The reason for this mismatch, which challenges our understanding of EHB evolution, is unclear.

4.2. Low-mass post-RGB binaries

Our sample contains two sdBs that might be good candidates for low-mass post-RGB stars. With a low effective temperature of $20\,500 \text{ K}$ and a rather high surface gravity $\log g = 5.52$ J083334.76-045759.4 is situated well below the EHB. Such a location is inconsistent with core-helium burning. Furthermore, it shows a high $\Delta RV_{\max} = 161 \text{ km s}^{-1}$. J094750.71+162731.8 is hotter ($T_{\text{eff}} = 30000 \text{ K}$), but has a very high surface gravity $\log g = 6.25$. Also situated below the EHB it shows $\Delta RV_{\max} = 130 \text{ km s}^{-1}$. However, whether a significant contribution of low-mass post-RGB binaries leads to the wider distribution of RV-shifts, still needs to be studied in more detail (see also discussion in Geier et al. 2013a).

4.3. Hierarchical triple systems

One sdB in our sample is a double-lined system and shows weak spectral features of a main-sequence companion. J205101.72+011259.7 shows a shift of $91.0 \pm 31.5 \text{ km s}^{-1}$ within just 0.0141 d with a false-detection probability of only 0.05%. It is very unlikely that this variation is caused by the main-sequence companion. The solved orbits of sdB+MS binaries have long periods of the order of 1000 d (Vos et al. 2012, 2013; Barlow et al. 2012, 2013). We therefore conclude that J205101.72+011259.7 is another candidate for a hierarchical triple system consisting of an sdB in a short-period binary with unseen companion and a main sequence star orbiting this inner binary with a long period (e.g. Barlow et al. 2014, see also discussion in Kupfer et al. 2015).

4.4. The fraction of massive compact companions

The primary aim of the MUCHFUSS project is to find massive compact companions to sdB stars. However, only two known sdB binaries with periods shorter than 0.1 d and $\Delta RV_{\max} \sim 700 \text{ km s}^{-1}$ have WD companions with masses exceeding $0.7 M_{\odot}$

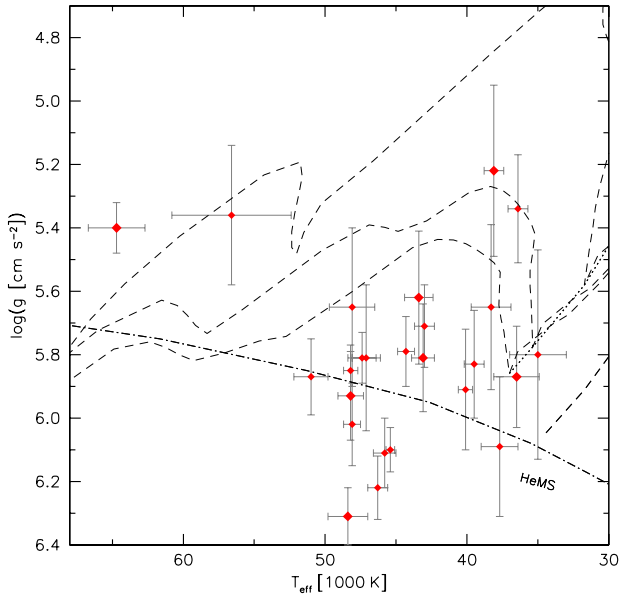


Fig. 6. $T_{\text{eff}} - \log g$ diagram of RV variable helium-rich sdOB and sdO stars (see Fig. 1). The size of the symbols scales with ΔRV_{max} . The helium main sequence (HeMS) and the HB band are superimposed with HB evolutionary tracks (dashed lines) for subsolar metallicity ($\log z = -1.48$) from Dorman et al. (1993). The three tracks correspond to helium core masses of 0.488, 0.490 and 0.495 M_{\odot} (from bottom-left to top-right).

(Geier et al. 2007, 2013b). SdB+NS/BH binaries with similar periods would have $\Delta RV_{\text{max}} > 1000 \text{ km s}^{-1}$.

However, the highest ΔRV_{max} measured in our subsample of hydrogen-rich sdB, sdOB and sdO stars is just 359 km s^{-1} (see Table 3). Due to the RV sampling of our dataset provided by the individual SDSS spectra it is very unlikely that we have missed a short-period (0.1 d) binary with an $\Delta RV_{\text{max}} > 1000 \text{ km s}^{-1}$ by chance. To estimate an upper limit for the fraction of such extremely close binary sdB+NS/BH binaries in our sample we count the number of hydrogen-rich sdBs and sdOBs with significant RV variability ($\log p < -4.0$) in our sample (76 objects, see Table 3) and invert it. In this way we derive the fraction of those objects in our sample to be smaller than 1.3%. This fraction is still consistent with the theoretically predicted fractions of about 1% (Yungelson et al. 2005; Geier et al. 2010b; Nelemans 2010).

However, we would most likely not expect the most massive compact companions in our sample to have such short orbital periods anyway. To allow the massive companion to spiral in deep enough to form such compact binaries during the common envelope phase, the red-giant progenitors of the sdB stars are predicted to have tightly bound envelopes and to be rather massive ($2 - 3 M_{\odot}$, Geier et al. 2013b). Such stars are only found in young field populations like the Galactic thin disk and the two sdB binaries with the most massive WD companions known so far indeed belong to this population (Maxted et al. 2000a; Geier et al. 2007; Geier et al. 2013b).

Fig. 5 shows the distribution of spectroscopic distances for the sample. Those distances range from 1 to more than 20 kpc. Taking into account that the SDSS footprint mostly covers high Galactic latitudes and assuming a scale-height of $\sim 0.3 \text{ kpc}$ for the thin disk, we conclude that the vast majority of the stars in

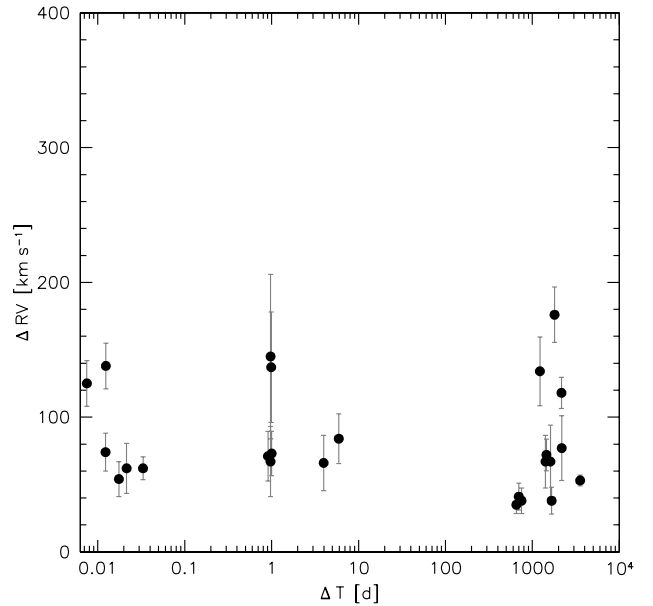


Fig. 7. Highest radial velocity shift between individual spectra plotted against time difference between the corresponding observing epochs for helium-rich sdO and sdOB stars (see Fig. 3).

our sample do not belong to this young population. Most binary candidates exceeding $d \sim 3 \text{ kpc}$ should belong to the old Galactic halo population, the rest to the intermediate thick disk population. Since both populations do not contain intermediate mass main-sequence stars, which are the likely progenitors of short-period sdBs with massive compact companions, it is no surprise that we do not find them in our sample.

While we can exclude sdB binaries with periods of a few hours and massive compact companions, our sample might still contain such objects with longer periods. Since more massive companions are expected to be quite efficient in ejecting the common envelope, such binaries might exist. Taking into account the ΔRV_{max} -distribution and the fraction of solved binary orbits (see Fig. 3), we estimate that a yet undetected population of long-period binaries with $K < 100 \text{ km s}^{-1}$ might be present. Assuming the canonical sdB mass of $0.47 M_{\odot}$ and a minimum companion mass at the Chandrasekhar limit ($1.4 M_{\odot}$) this translates into orbital periods longer than $\sim 8 \text{ d}$.

4.5. Irregular RV variations of helium-rich hot subdwarf stars

Our RV-variable sample contains 29 helium-rich hot subdwarf stars. 14 of them show significant RV variations while 15 qualify as candidates (see Table 4). Most of them are situated close to the He-MS in the $T_{\text{eff}} - \log g$ -diagram (see Fig. 6) and the atmospheric parameters are quite typical for the field population of He-sdOs ($T_{\text{eff}} = 40\,000 - 50\,000 \text{ K}$, Ströer et al. 2007; Nemeth et al. 2012). However, quite a number of stars have lower temperatures between $35\,000 \text{ K}$ and $40\,000 \text{ K}$. Those helium-rich sdOBs are rare in the field population, but quite dominant in the globular cluster $\omega \text{ Cen}$ (Latour et al. 2014). Following the discussion in Latour et al. (2014) this might be related to the age of the parent population, since most of the stars in our sample belong to the old thick disk or halo populations, while most of the bright stars studied by Nemeth et al. (2012) belong to the young

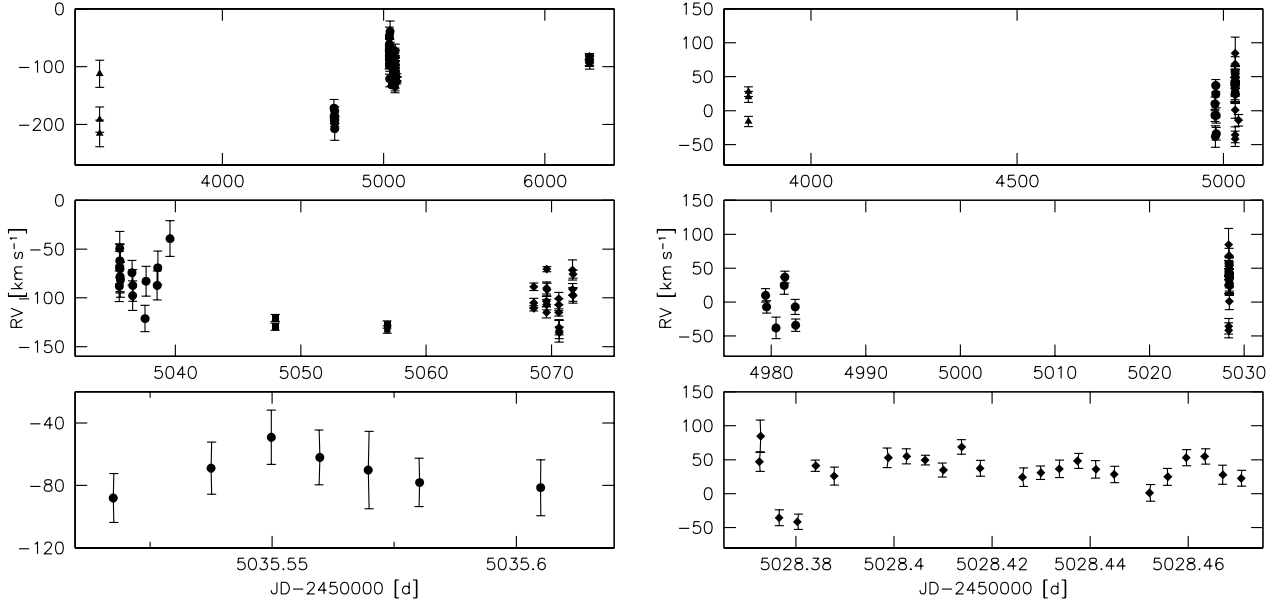


Fig. 8. Radial velocities of J232757.46+483755.2 (left panels) and J141549.05+111213.9 (right panels) against Julian date. Significant variations are present on timescales of years (upper panels), days (middle panels) and hours (lower panels).

thin disk population. The He-sdOs J232757.46+483755.2 and J110215.45+024034.1 seem to be more evolved than the rest of the sample and might also be associated to the helium-rich post-AGB stars.

J160450.44+051909.2 and J160623.21+363005.4 belong to the class of He-sdOBs with lower surface gravity (e.g. Naslim et al. 2010).³ Only one He-sdOB is known to be in a close double-lined, spectroscopic binary with an almost identical companion of the same type (Sener & Jeffery 2014). Another close binary contains an sdB with intermediate helium-enrichment (Naslim et al. 2012). Follow-up observations are needed to study the binary properties of those rare objects and compare them with the other hot subdwarf populations.

The discovery of RV variable He-sdOs (Green et al. 2008; Geier et al. 2011a) on the other hand seemed to be inconsistent with the idea, that those stars are formed by He-WD mergers (e.g. Webbink 1984), because merger products are expected to be single stars. Fig. 7 shows the maximum RV shifts between individual spectra plotted against the time difference between the corresponding epochs. When compared with Fig. 3 one can see that there are no stars with shifts higher than $\sim 200 \text{ km s}^{-1}$ and that the number of objects showing shifts at short timespans ($< 0.1 \text{ d}$) is smaller as well.

Because of the important implications for their formation, we were eager to solve the first He-sdO binaries and gave them high priority in our follow-up campaign. However, although we gathered up to 59 epochs for some of them, we were not able to find a single orbital solution. Adding more data in general degraded preliminary solutions that looked promising. Besides assuming circular orbits we also allowed for eccentricity and explored especially the parameter space of high orbital eccentricities (see Geier et al. 2011b). No periodic variations could be detected with sufficient significance.

³ In the literature those objects are usually called He-sdBs, but here we follow the more detailed spectroscopic classification outlined in Sect. 3.2.

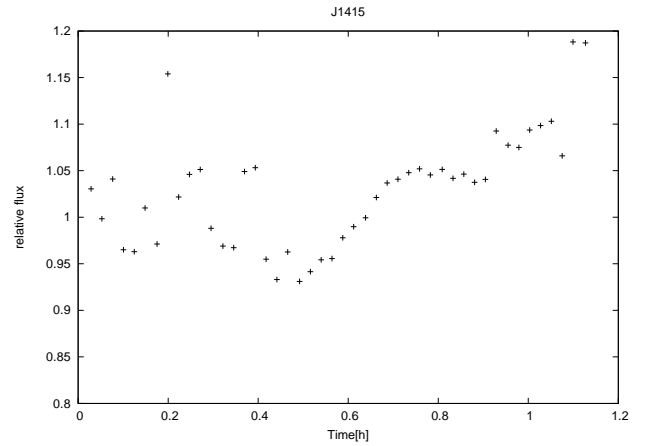


Fig. 9. V_B -band lightcurve of J141549.05+111213.9 taken with the BUSCA camera mounted at the 2.2m telescope at Calar Alto (Schaffenroth et al. in prep.).

Fig. 8 shows the radial velocities of the two He-sdO stars J141549.05+111213.9 and J232757.46+483755.2 for which we obtained the most data. Significant RV variations with amplitudes of up to $\sim 180 \text{ km s}^{-1}$ are seen on timescales of years, days and even hours. While J141549.05+111213.9 has atmospheric parameters typical for He-sdO stars, J232757.46+483755.2 has a higher effective temperature and seems to be more evolved (see Table 3, Fig. 6).

The origin of these irregular RV variations remains unclear. Østensen et al. (2010) reported the discovery of irregular variations in the light curve of the He-sdOB star J19352+4555 observed by the Kepler mission. Jeffery et al. (2013) found another He-sdOB star with Kepler light curves (KIC 10449976) that shows a variation with a period of 3.9d and variable amplitude. Radial velocity follow-up with time-resolved spec-

troscopy revealed a possible, but still marginal RV variability of $50 \pm 20 \text{ km s}^{-1}$. Most recently, Green et al. (2014) reported irregular variations in the lightcurves of two helium-rich and one hydrogen-rich sdO star. They also found RV variations of up to 20 km s^{-1} for some hydrogen- and helium-rich sdO stars.

During our photometric follow-up campaign (Schaffenroth et al. in prep.) we obtained a light curve of J141549.05+111213.9 (see Fig. 9) showing irregular variations very similar to the ones found by Green et al. (2014). There might therefore be a link between those two phenomena. A similar light curve of J232757.46+483755.2 showed no such variations, but this might also be an indication for their transient nature. It remains to be seen whether the high RV variations we found are really connected to the light curve variations observed in similar stars.

Whether this behaviour is restricted to helium-rich sdOs only or might also affect hydrogen-rich sdOs is unclear. The possibly connected photometric variations discovered by Green et al. (2014) affect both kinds of sdOs. Also the distributions of maximum RV-shifts for both populations look quite similar (see Fig. 3 right panel, Fig. 7). However, since we focused our follow-up mostly on hydrogen-rich sdBs and helium-rich sdOs, we did not obtain a sufficient number of RVs to check for irregular variations in one of the hydrogen-rich sdOs. An important difference between the two populations is that at least some hydrogen-rich sdOs are known to reside in close binaries (see Kupfer et al. 2015 and references therein), whereas not a single He-sdO in a close binary system has been found yet.

Some ideas have been put forward to explain the light curve variations. Jeffery et al. (2013) suggested that the variations might be due to star spots caused by magnetic fields. They also discuss the possibility of a shallow reflection effect originating from the irradiated hemisphere of a cool low-mass companion. Bear & Soker (2014) propose a heated planetary companion with strong weather to be responsible for the variability of KIC 10449976. Green et al. (2014) see strong similarities of the variations detected in their stars to the variations seen in some cataclysmic variables and attribute them to the presence of accretion disks. The high and irregular RV variations seen in our objects can be hardly explained in those ways. A reflection effect binary with a low-mass companion should show periodic variations with small RV amplitudes and the presence of an accretion disk would require a close companion as well.

Another possible reason might be magnetic activity of those stars. Heber et al. (2013) reported the discovery of a He-sdO star with significant Zeeman-splitting and a magnetic field of several hundred kG. More of those objects have been discovered recently (Nemeth priv. comm.). Variable magnetic fields might lead to distortions of the spectral lines, which are not resolved in the medium-resolution spectra we have and may mimic irregular RV shifts. However, the very high RV shifts observed are again hardly consistent with such a scenario. High-resolution, time-resolved follow-up photometry, spectroscopy, and maybe also spectropolarimetry are necessary to study those mysterious RV shifts.

5. Summary

In this paper we provide classifications, atmospheric parameters and a complete RV catalogue containing 1914 single measurements of the 177 most likely RV variable hot subluminoous stars discovered in the MUCHFUSS project from SDSS DR7.

We detect a mismatch between the ΔRV_{max} -distribution of the sdB and the more evolved sdOB and sdO stars, which

challenges our understanding of their evolutionary connection. Our sample contains two candidates for He-WD progenitors. Furthermore, one of the RV variable sdB binaries is double-lined and a candidate for a hierarchical triple system.

Based on the ΔRV_{max} -distribution of the hydrogen-rich sdB and sdOB stars we constrain the fraction of close massive compact companions in our sample to be smaller than $\sim 1.3\%$. However, the sample might still contain such binaries with longer periods exceeding $\sim 8 \text{ d}$. Future studies should therefore concentrate on this parameter range.

Irregular RV variations of unknown origin with amplitudes of up to $\sim 180 \text{ km s}^{-1}$ on timescales of years, days and even hours have been detected in some He-sdO stars. They might be connected to irregular photometric variations in some cases.

Acknowledgements. T.R.M. acknowledges support from the UK's Science and Technology Facilities Council, grant ST/L000733/1. E.Z. and C.H. are supported by the Deutsche Forschungsgemeinschaft (DFG) through grants HE1356/45-2 and HE1356/62-1. T.K. acknowledges support by the Netherlands Research School for Astronomy (NOVA). V.S. is supported by Deutsches Zentrum für Luft- und Raumfahrt (DLR) under grant 50 OR 1110.

Based on observations at the La Silla-Paranal Observatory of the European Southern Observatory for programmes number 165.H-0588(A), 079.D-0288(A), 080.D-0685(A), 081.D-0819, 082.D-0649, 084.D-0348, 089.D-0265(A), 090.D-0012(A), 091.D-0038(A) and 092.D-0040(A).

Based on observations collected at the Centro Astronómico Hispano Alemán (CAHA) at Calar Alto, operated jointly by the Max-Planck Institut für Astronomie and the Instituto de Astrofísica de Andalucía (CSIC).

Based on observations with the William Herschel and Isaac Newton Telescopes operated by the Isaac Newton Group at the Observatorio del Roque de los Muchachos of the Instituto de Astrofísica de Canarias on the island of La Palma, Spain.

Based on observations with the Southern Astrophysical Research (SOAR) telescope operated by the U.S. National Optical Astronomy Observatory (NOAO), the Ministério da Ciência e Tecnologia of the Federal Republic of Brazil (MCT), the University of North Carolina at Chapel Hill (UNC), and Michigan State University (MSU).

Based on observations obtained at the Gemini Observatory, which is operated by the Association of Universities for Research in Astronomy, Inc., under a cooperative agreement with the NSF on behalf of the Gemini partnership: the National Science Foundation (United States), the Science and Technology Facilities Council (United Kingdom), the National Research Council (Canada), CONICYT (Chile), the Australian Research Council (Australia), Ministério da Ciência e Tecnologia (Brazil) and Ministerio de Ciencia, Tecnología e Innovación Productiva (Argentina).

Funding for the SDSS and SDSS-II has been provided by the Alfred P. Sloan Foundation, the Participating Institutions, the National Science Foundation, the U.S. Department of Energy, the National Aeronautics and Space Administration, the Japanese Monbukagakusho, the Max Planck Society, and the Higher Education Funding Council for England. The SDSS Web Site is <http://www.sdss.org/>.

The SDSS is managed by the Astrophysical Research Consortium for the Participating Institutions. The Participating Institutions are the American Museum of Natural History, Astrophysical Institute Potsdam, University of Basel, University of Cambridge, Case Western Reserve University, University of Chicago, Drexel University, Fermilab, the Institute for Advanced Study, the Japan Participation Group, Johns Hopkins University, the Joint Institute for Nuclear Astrophysics, the Kavli Institute for Particle Astrophysics and Cosmology, the Korean Scientist Group, the Chinese Academy of Sciences (LAMOST), Los Alamos National Laboratory, the Max-Planck-Institute for Astronomy (MPIA), the Max-Planck-Institute for Astrophysics (MPA), New Mexico State University, Ohio State University, University of Pittsburgh, University of Portsmouth, Princeton University, the United States Naval Observatory, and the University of Washington.

References

- Abazajian, K., Adelman-McCarthy, J. K., Agüeros, M. A., et al. 2009, *ApJS*, 182, 543
- Ahmad, A., Jeffery, C. S., & Fullerton, A. W. 2004, *A&A*, 418, 275
- Althaus, L. G., Panei, J. A., Miller Bertolami, M. M., et al. 2009, *ApJ*, 704, 1605
- Barlow, B. N., Wade, R. A., Liss, S. E., Østensen, R. H., & van Winckel, H. 2012, *ApJ*, 758, 58
- Barlow, B. N., Liss, S. E., Wade, R. A., & Green, E. M. 2013, *ApJ*, 771, 23

- Barlow, B. N., Wade, R., Liss, S., & Stark, M. 2014, ASP Conf. Ser., 481, 301
- Geier, S., & Soker, N. 2014, MNRAS, 437, 1400
- Brown, W. R., Kilic, M., Allende Prieto, C., Gianninas, A., & Kenyon, S. 2012, 744, 142
- Copperwheat, C., Morales-Rueda, L., Marsh, T. R., et al. 2011, MNRAS, 415, 1381
- Dorman, B., Rood, R. T., & O’Connell, R. W. 1993, ApJ, 419, 596
- Driebe, T., Schönberner, D., Bloecker, T., & Herwig, F. 1998, A&A, 339, 123
- Drilling, J. S., Jeffery, C. S., Heber, U., Moehler, S., & Napiwotzki, R. 2013, A&A, 551, 31
- Edelmann, H., Heber, U., Altmann, M., Karl, C., & Lisker, T. 2005, A&A, 442, 1023
- Edelmann, H., Heber, U., Hagen, H.-J., et al. 2003, A&A, 400, 939
- Fontaine, G., Brassard, P., Charpinet, S., et al. 2012, A&A, 539, 12
- Geier, S., Nesslinger, S., Heber, U., et al. 2007, A&A, 464, 2990
- Geier, S., Nesslinger, S., Heber, U., et al. 2008, A&A, 477, L13
- Geier, S., Heber, U., Kupfer, T., & Napiwotzki, R. 2010a, A&A, 515, 37
- Geier, S., Heber, U., Podsiadlowski, Ph., et al. 2010b, A&A, 519, 25
- Geier, S., Hirsch, H., Tillich, A., et al. 2011a, A&A, 530, 28
- Geier, S., Maxted, P. F. L., Napiwotzki, R., et al. 2011b, A&A, 526, 39
- Geier, S., Schaffenroth, V., Drechsel, H., et al. 2011c, ApJ, 731, L22
- Geier, S. 2013, EPJ Web of Conferences, 43, 04001
- Geier, S., Heber, U., Edelmann, H., et al. 2013a, A&A, 557, 122
- Geier, S., Marsh, T. R., Wang, B., et al. 2013b, A&A, 554, 54
- Geier, S., Østensen, R. H., Heber, U., et al. 2014, A&A, 562, 95
- Geier, S., Kupfer, T., Schaffenroth, V., et al. 2015, A&A, in prep.
- Green, E. M., Fontaine, G., Hyde, E. A., For, B.-Q., & Chayer, P. 2008, ASP Conf. Ser., 392, 75
- Green, E. M., Johnson, C. B., Wallace, S. C., et al. 2014, ASP Conf. Ser., 481, 161
- Han, Z. 2008, A&A, 484, L31
- Han, Z., Podsiadlowski, P., Maxted, P. F. L., Marsh, T. R., & Ivanova, N. 2002, MNRAS, 336, 449
- Han, Z., Podsiadlowski, P., Maxted, P. F. L., & Marsh, T. R. 2003, MNRAS, 341, 669
- Heber, U. 1986, A&A, 155, 33
- Heber, U. 2009, ARA&A, 47, 211
- Heber, U., Edelmann, H., Lisker, T., & Napiwotzki, R. 2003, A&A, 411, 477
- Heber, U., Geier, S., & Gänsicke, B. T. 2013, EPJ Web of Conferences, 43, 04002
- Heber, U., & Hirsch, H. 2010, AIP Conf. Ser., 1314, 79
- Hirsch, H. 2009, PhD thesis, Friedrich-Alexander University Erlangen-Nürnberg
- Hirsch, H., & Heber, U. 2009, JPhCS, 172, 2015
- Iben, I., & Tutukov, A. V. 1984, ApJ, 284, 719
- Jeffery, C. S. 2008, ASP Conf. Ser., 391, 3
- Jeffery, C. S., Ramsay, G., Naslim, N., et al. 2013, MNRAS, 429, 3207
- Kaplan, D. L., Bhalerao, V. B., van Kerkwijk, M. H., et al. 2013, ApJ, 765, 158
- Kleinman, S. J. 2010, AIP Conf. Ser., 1237, 156
- Kupfer, T., Geier, S., Schaffenroth, V., et al. 2015, A&A, in press (arXiv:1501.07760)
- Lanz, T., Brown, T. M., Sweigart, A. V., Hubeny, I., & Landsman, W. B. 2004, ApJ, 602, 342
- Latour, M., Randall, S. K., Fontaine, G., et al. 2014, ApJ, 795, 106
- Lisker, T., Heber, U., Napiwotzki, R., Christlieb, N., Han, Z., et al. 2005, A&A, 430, 223
- Maxted, P. F. L., Heber, U., Marsh, T. R., & North, R. C. 2001, MNRAS, 326, 139
- Maxted, P. F. L., Marsh, T. R., & North, R. C. 2000a, MNRAS, 317, L41
- Miller Bertolami, M. M., Althaus, L. G., Unglaub, K., & Weiss, A. 2008, A&A, 491, 253
- Moehler, S., Richtler, T., de Boer, K. S., Dettmar, R. J., & Heber, U. 1990, A&AS, 86, 53
- Morales-Rueda, L., Maxted, P. F. L., Marsh, T. R., North, R. C., & Heber, U. 2003a, MNRAS, 338, 752
- Napiwotzki, R., Yungelson, L., Nelemans, G. et al. 2004, ASP Conf. Ser., 318, 402
- Napiwotzki, R. 2008, ASP Conf. Ser., 392, 139
- Naslim, N., Jeffery, C. S., Ahmad, S., Behara, N. T., & Sahin, T. 2010, MNRAS, 409, 582
- Naslim, N., Geier, S., Jeffery, C. S., et al. 2012, MNRAS, 423, 3031
- Nelemans, G. 2010, Ap&SS, 329, 25
- Nemeth, P., Kawka, A., & Vennes, S. 2012, MNRAS, 427, 2180
- Østensen, R. H., Silvotti, R., Charpinet, S., et al. 2010, MNRAS, 409, 1470
- Østensen, R. H., Degroote, P., Telting, J. H., et al. 2012, ApJ, 753, L17
- Østensen, R. H., Geier, S., Schaffenroth, V., et al. 2013, A&A, 559, 35
- O’Toole, S. J., Heber, U., Jeffery, S. J., et al. 2005, A&A, 440, 667
- O’Toole, S. J., & Heber, U. 2006, A&A, 452, 579
- Pfahl, E., Rappaport, S., & Podsiadlowski, Ph. 2003, ApJ, 597, 1036
- Podsiadlowski, Ph., Rappaport, S., & Pfahl, E. D. 2002, ApJ, 565, 1107
- Ramspeck, M., Heber, U., & Edelmann, H. 2001, A&A, 379, 235
- Rebassa-Mansergas, A., Gänsicke, B. T., Rodríguez-Gil, P., Schreiber, M. R., & Koester, D. 2007, MNRAS, 382, 1377
- Reindl, N., Geier, S., Kupfer, T., et al. 2015, A&A, in prep.
- Schaffenroth, V., Geier, S., Heber, U., et al. 2014, A&A, 564, 98
- Schaller, G., Schaerer, D., Meynet, G., & Maeder, A. 1992, A&AS, 96, 269
- Schönberner, D. 1983, ApJ, 272, 708
- Sener, H. T., & Jeffery, C. S. 2014, MNRAS, 440, 2676
- Silvotti, R., Østensen, R. H., Bloemen, S., et al. 2012, MNRAS, 424, 1752
- Ströer, A., Heber, U., Lisker, T., et al. 2007, A&A, 462, 269
- Tillich, A., Heber, U., Geier, S., et al. 2011, A&A, 527, 137
- Tutukov, A. V., & Yungelson, L. R. 1981, Nauchnye Informatsii, 49, 3
- Vennes, S., Kawka, A., O’Toole, S. J., Németh, P., & Burton, D. 2012, ApJ, 759, L25
- Vos, J., Østensen, R. H., Degroote, P., et al. 2012, A&A, 548, 6
- Vos, J., Østensen, R. H., Nemeth, P., et al. 2013, A&A, 559, 54
- Webbink, R. F. 1984, ApJ, 277, 355
- Werner, K., Rauch, T., & Kepler, S. O. 2014, A&A, 564, 53
- Yoon, S.-C., & Langer, N. 2004, A&A, 419, 645
- Yungelson, L. R., & Tutukov, A. V. 2005, ARep, 49, 871
- Zhang, X., & Jeffery, C. S. 2012, MNRAS, 419, 452

Appendix A: Appendix

Table 3. Parameters of 139 hydrogen-rich hot subdwarfs (89 RV variable, 50 RV variable candidates). Solved binaries are marked in bold face and their orbital parameters can be found in Kupfer et al. (2015) and references therein.

Name	Class	m_V [mag]	T_{eff} [K]	$\log g$	$\log y$	d [kpc]	Δt [d]	ΔRV_{max} [km s $^{-1}$]	N	$\log p$
J082332.09+113641.9^b	sdB	16.7	31200 ± 600	5.79 ± 0.06	-2.0 ± 0.1	2.6 $^{+0.2}_{-0.2}$	53.9447	359.0 ± 6.5	22	< -680
J113840.68-003531.7^c	sdB	14.5	31200 ± 600	5.54 ± 0.09	< -3.0	1.2 $^{+0.2}_{-0.1}$	3361.5592	332.0 ± 14.0	31	< -680
J165404.26+303701.8^c	sdB	15.4	24900 ± 800	5.39 ± 0.12	-2.4 ± 0.1	1.8 $^{+0.3}_{-0.3}$	2.9365	271.0 ± 17.0	38	< -680
J225638.34+065651.1^c	sdB	15.3	28500 ± 500	5.64 ± 0.05	-2.3 ± 0.2	1.5 $^{+0.1}_{-0.1}$	42.3494	269.0 ± 14.0	50	< -680
J172624.10+274419.3^c	sdB	16.0	32600 ± 500	5.84 ± 0.05	-2.2 ± 0.1	1.9 $^{+0.1}_{-0.1}$	55.9741	263.0 ± 12.0	38	< -680
J150513.52+110836.6^c	sdB	15.4	33200 ± 500	5.80 ± 0.10	-2.3 ± 0.1	1.5 $^{+0.2}_{-0.1}$	43.6564	222.0 ± 8.0	42	< -680
J134632.66+281722.7^b	sdB	14.9	28800 ± 600	5.46 ± 0.07	-2.6 ± 0.2	1.6 $^{+0.2}_{-0.1}$	0.9988	191.0 ± 7.0	41	< -680
J002323.99-002953.2^c	sdB	15.5	29200 ± 500	5.69 ± 0.05	-2.0 ± 0.1	1.6 $^{+0.1}_{-0.1}$	1.0413	168.0 ± 4.0	47	< -680
J083006.17+475150.4^b	sdB	16.0	25300 ± 600	5.38 ± 0.06	< -3.0	2.5 $^{+0.2}_{-0.7}$	4405.6747	164.0 ± 9.0	37	< -680
J095238.93+625818.9^b	sdB	14.8	27700 ± 600	5.59 ± 0.06	-2.6 ± 0.1	1.2 $^{+0.1}_{-0.1}$	1183.7390	154.0 ± 8.0	34	< -680
J162256.66+473051.1^d	sdB	16.2	29000 ± 600	5.65 ± 0.06	-1.9 ± 0.1	2.3 $^{+0.2}_{-0.2}$	1.9832	135.0 ± 4.5	34	< -680
J012022.94+395059.4^e	sdB	15.4	28500 ± 100	5.42 ± 0.01	-3.0 ± 0.1	2.1 $^{+0.0}_{-0.0}$	1358.9782	129.0 ± 6.5	22	< -680
J173606.25+315842.7	sdB	17.0	31300 ± 300	5.87 ± 0.09	-2.5 ± 0.2	2.8 $^{+0.3}_{-0.0}$	1567.7104	195.0 ± 12.0	12	-537.49
J032138.67+053840.0^b	sdB	15.0	30700 ± 500	5.74 ± 0.06	-2.4 ± 0.1	1.3 $^{+0.1}_{-0.1}$	1699.1435	110.0 ± 9.0	46	-536.46
J191908.76+371423.9	sdB	17.2	28300 ± 400	5.69 ± 0.10	-2.7 ± 0.3	3.4 $^{+0.5}_{-0.4}$	68.8608	237.0 ± 12.0	15	-526.21
J102151.64+301011.9^a	sdB	18.3	30700 ± 500	5.71 ± 0.06	< -3.0	5.8 $^{+0.5}_{-0.3}$	14.9363	277.0 ± 37.0	19	-508.16
J204613.40-045418.7^c	sdB	16.2	31600 ± 500	5.54 ± 0.08	< -3.0	2.8 $^{+0.3}_{-0.3}$	286.2265	259.0 ± 16.0	22	-480.28
J173806.51+451701.7	sdB	17.4	30500 ± 500	5.40 ± 0.08	< -3.0	5.5 $^{+0.6}_{-0.6}$	1.9536	233.0 ± 8.5	13	-461.58
J183249.04+630910.7^b	sdB	15.8	26800 ± 700	5.29 ± 0.09	-2.6 ± 0.1	2.7 $^{+0.4}_{-0.3}$	1487.7733	141.0 ± 8.0	17	-453.62
J164326.04+330113.1 ^a	sdB	16.3	27900 ± 500	5.62 ± 0.07	-2.3 ± 0.2	2.4 $^{+0.2}_{-0.3}$	2.8085	175.0 ± 5.5	10	-452.26
J011857.19-002546.5^b	sdB	14.9	27900 ± 600	5.55 ± 0.07	< -3.0	1.3 $^{+0.1}_{-0.1}$	265.2187	140.0 ± 8.0	43	-386.44
J192059.78+372220.0 ^f	sdB	15.8	27600 ± 600	5.40 ± 0.10	-2.5 ± 0.3	2.4 $^{+0.3}_{-0.3}$	1.9589	123.0 ± 4.5	15	-319.72
J150829.02+494050.9^b	sdB	17.7	29600 ± 600	5.73 ± 0.07	-2.3 ± 0.1	4.3 $^{+0.5}_{-0.4}$	2161.9292	209.0 ± 15.5	58	-269.10
J180940.41+234328.4	sdB	16.5	28500 ± 300	5.44 ± 0.06	-2.9 ± 0.2	3.3 $^{+0.4}_{-0.3}$	2909.9029	342.0 ± 29.5	36	-215.11
J183349.79+652056.3	sdB	17.4	27200 ± 500	5.56 ± 0.12	-2.6 ± 0.1	4.1 $^{+0.7}_{-0.6}$	68.8591	177.0 ± 9.5	16	-190.20
J095101.28+034757.0^b	sdB	15.9	29800 ± 300	5.48 ± 0.04	-2.8 ± 0.3	2.5 $^{+0.1}_{-0.1}$	1.0425	183.0 ± 13.0	31	-170.79
J082053.53+000843.4^g	sdB	15.2	26700 ± 900	5.48 ± 0.10	-2.0 ± 0.1	1.6 $^{+0.3}_{-0.3}$	388.9794	99.0 ± 11.5	24	-153.08
J080738.96-083322.6	sdB	17.2	27600 ± 600	5.61 ± 0.17	-2.7 ± 0.3	3.6 $^{+0.9}_{-0.7}$	0.0736	298.0 ± 19.0	27	-136.25
J152222.15-013018.3^b	sdB	17.8	25200 ± 700	5.47 ± 0.09	< -3.0	5.2 $^{+0.7}_{-0.6}$	3.0055	173.0 ± 30.0	26	-126.07
J155628.34+011335.0 ^a	sdB	16.2	32700 ± 600	5.51 ± 0.08	-2.9 ± 0.2	3.1 $^{+0.4}_{-0.3}$	4412.8910	118.0 ± 10.5	15	-121.64
J113241.58-063652.8^b	sdO	16.2	46400 ± 1000	5.89 ± 0.07	-2.9 ± 0.2	2.4 $^{+0.3}_{-0.2}$	1517.8240	103.0 ± 10.0	32	-108.89
J222850.00+391917.4	sdB	16.4	33500 ± 900	5.80 ± 0.10	-1.7 ± 0.1	2.4 $^{+0.4}_{-0.3}$	2051.8410	104.0 ± 7.5	40	-85.63
J173057.94+320737.0	sdB	16.2	28200 ± 700	5.40 ± 0.05	-2.9 ± 0.2	3.0 $^{+0.2}_{-0.3}$	1.9680	94.0 ± 8.0	6	-69.42
J083334.76-045759.4	sdB	18.2	20500 ± 700	5.52 ± 0.10	< -3.0	5.0 $^{+0.8}_{-0.7}$	14.8908	161.0 ± 8.5	11	-66.11
J164853.26+121703.0	sdB	18.5	30400 ± 500	5.38 ± 0.11	< -3.0	9.3 $^{+1.4}_{-1.2}$	0.0684	135.0 ± 13.0	11	-64.89
J072245.27+305233.4	sdB	18.0	25900 ± 700	5.61 ± 0.16	-2.6 ± 0.2	5.0 $^{+1.2}_{-0.9}$	1.0019	123.0 ± 12.0	7	-62.09
J093059.63+025032.3	sdB	15.0	30000 ± 600	5.67 ± 0.18	-2.7 ± 0.2	1.3 $^{+0.3}_{-0.3}$	2986.7695	91.0 ± 9.0	10	-49.22
J203526.46+141948.4	sdB	18.7	30200 ± 600	5.57 ± 0.07	-2.9 ± 0.2	8.3 $^{+0.9}_{-0.8}$	1.0235	163.0 ± 25.5	12	-33.12
J203843.97+141706.0	sdOB	18.7	36800 ± 1000	5.89 ± 0.20	-2.4 ± 0.3	6.8 $^{+1.9}_{-1.5}$	0.9067	102.0 ± 10.5	12	-32.22
J095229.62+301553.6 ^a	sdOB	18.5	35200 ± 1200	5.05 ± 0.17	< -3.0	16.0 $^{+3.8}_{-3.3}$	1155.7612	198.0 ± 27.5	5	-28.52
J154531.01+563944.7	sdB	17.0	26200 ± 900	5.13 ± 0.14	-2.0 ± 0.2	5.5 $^{+1.3}_{-1.0}$	2527.7769	70.0 ± 8.5	9	-27.76
J200959.27-115519.9	sdB	18.7	29700 ± 700	5.31 ± 0.08	< -3.0	10.7 $^{+1.3}_{-1.2}$	1.9832	156.0 ± 23.0	8	-27.48
J005107.01+004232.5	sdOB	15.9	38500 ± 300	5.83 ± 0.07	-1.0 ± 0.1	2.0 $^{+0.2}_{-0.2}$	2.0256	54.0 ± 6.5	7	-24.96
J104248.94+033355.3	sdO	17.6	41200 ± 3200	4.83 ± 0.15	-2.1 ± 0.4	14.5 $^{+3.4}_{-2.8}$	2246.6948	49.0 ± 5.0	2	-24.34
J181141.86+241902.7	sdB	18.7	-	-	-	-	0.9972	248.0 ± 26.0	7	-23.56
J071424.12+401645.9	sdB	18.2	27700 ± 700	5.38 ± 0.11	-2.6 ± 0.1	7.6 $^{+1.2}_{-1.1}$	2.9312	152.0 ± 24.0	9	-23.37
J204300.90+002145.0 ^a	sdO	17.9	40200 ± 700	6.15 ± 0.13	-1.3 ± 0.4	3.6 $^{+0.6}_{-0.4}$	18.8480	65.0 ± 6.5	9	-22.54
J191645.87+371224.5	sdB	18.3	33200 ± 1000	5.84 ± 0.17	-2.7 ± 0.2	5.6 $^{+1.4}_{-1.1}$	3.0338	134.0 ± 23.5	19	-22.15
J094750.71+162731.8	sdB	17.4	30000 ± 700	6.25 ± 0.31	-2.2 ± 0.3	2.1 $^{+1.0}_{-0.7}$	0.8902	130.0 ± 13.5	5	-20.08
J115358.81+353929.0 ^a	sdOB	16.6	29400 ± 500	5.49 ± 0.06	-2.5 ± 0.3	3.3 $^{+0.3}_{-0.3}$	1151.6544	79.0 ± 9.5	5	-19.15
J175125.67+255003.5 ^a	sdB	17.4	30600 ± 500	5.48 ± 0.08	< -3.8	5.0 $^{+0.5}_{-0.5}$	1533.6229	72.0 ± 10.0	8	-16.50
J125702.30+435245.8 ^a	sdB	18.2	28000 ± 1100	5.77 ± 0.17	< -3.0	4.9 $^{+1.3}_{-1.0}$	0.0098	63.0 ± 16.5	3	-16.32
J165446.26+182224.6	sdB	18.6	30100 ± 500	5.50 ± 0.08	-1.7 ± 0.1	8.5 $^{+1.0}_{-0.9}$	1396.0335	48.0 ± 5.5	3	-15.27
J120855.51+403716.1	sdB	18.6	34100 ± 900	5.98 ± 0.13	-1.5 ± 0.1	5.4 $^{+1.0}_{-0.9}$	0.0260	171.0 ± 20.0	7	-14.61
J164122.32+334452.0	sdB	15.5	28200 ± 500	5.49 ± 0.11	-2.5 ± 0.3	1.9 $^{+0.3}_{-0.3}$	2213.5393	77.0 ± 8.0	8	-14.60
J211421.39+100411.4	sdOB	18.4	36100 ± 900	5.48 ± 0.13	-2.5 ± 0.3	9.2 $^{+1.6}_{-1.4}$	1427.1132	69.0 ± 12.0	7	-14.02
J170810.97+244341.6 ^a	sdOB	18.5	35600 ± 800	5.58 ± 0.14	-0.8 ± 0.1	8.5 $^{+1.6}_{-1.4}$	0.0125	160.0 ± 26.0	3	-13.73
J153411.10+543345.2 ^a	sdOB	16.9	34800 ± 700	5.64 ± 0.09	-2.6 ± 0.3	3.8 $^{+0.4}_{-0.4}$	0.0184	83.0 ± 18.5	8	-12.52
J224518.65+220746.5	sdB	16.6	34000 ± 800	5.82 ± 0.07	-2.2 ± 0.1	2.6 $^{+0.3}_{-0.3}$	1080.8857	70.0 ± 11.5	9	-12.28
J120613.40+205523.1	sdOB	18.4	35000 ± 500	5.35 ± 0.07	< -3.0	10.5 $^{+1.0}_{-0.9}$	2.9112	91.0 ± 23.5	10	-11.37
J204247.51+001913.9 ^b	sdB	19.6	34200 ± 400	5.89 ± 0.08	-1.3 ± 0.1	9.6 $^{+1.1}_{-1.0}$	1393.1941	69.0 ± 10.0	3	-10.83
J151314.23+234248.8	sdB	17.1	28700 ± 300	5.69 ± 0.10	-2.3 ± 0.2	3.3 $^{+0.4}_{-0.4}$	2.0006	58.0 ± 8.5	3	-10.83
J082944.75+132302.5	sdOB	17.2	39700 ± 600	5.42 ± 0.04	< -3.0	6.1 $^{+0.3}_{-0.3}$	24.9992	90.0 ± 16.5	5	-10.40

Name	Class	m_V [mag]	T_{eff} [K]	$\log g$	$\log y$	d [kpc]	Δt [d]	ΔRV_{max} [km s $^{-1}$]	N	$\log p$
J074534.16+372718.5 ^a	sdB	17.9	37500 ± 500	5.90 ± 0.09	< -3.0	4.6 ^{+0.5} _{-0.5}	0.0363	64.0 ± 17.0	8	-9.74
J202313.83+131254.9 ^a	sdB	17.2	29600 ± 600	5.64 ± 0.14	-2.1 ± 0.1	3.8 ^{+0.7} _{-0.6}	1201.7981	123.0 ± 19.0	5	-9.20
J162610.34+130401.6	sdB	19.4	33900 ± 500	5.63 ± 0.10	-1.0 ± 0.1	12.1 ^{+1.7} _{-1.5}	780.7541	51.0 ± 8.0	3	-9.16
J030607.95+382335.7 ⁱ	sdO	16.8	30100 ± 300	5.64 ± 0.03	-2.1 ± 0.1	3.2 ^{+0.1} _{-0.1}	2210.7452	48.0 ± 6.5	8	-8.85
J204451.08-062753.8	sdO	20.0	57100 ± 5200	5.61 ± 0.15	-2.2 ± 0.4	21.4 ^{+5.1} _{-4.2}	1087.0571	62.0 ± 10.5	3	-7.88
J091615.49+132833.1	sdB	17.5	30900 ± 400	5.48 ± 0.05	< -3.0	5.4 ^{+0.4} _{-0.4}	0.9512	55.0 ± 11.5	3	-7.58
J163413.09+163109.5	sdB	18.3	34600 ± 900	4.73 ± 0.12	-2.0 ± 0.5	20.7 ^{+3.5} _{-3.1}	1105.3751	21.0 ± 5.5	3	-7.44
J123220.09+260913.3	sdB	18.1	33700 ± 1100	5.40 ± 0.16	-1.3 ± 0.2	8.5 ^{+2.0} _{-1.7}	1.0302	134.0 ± 27.0	5	-7.36
J185129.02+182358.8	sdB	16.8	27800 ± 700	5.38 ± 0.10	< -3.0	3.9 ^{+0.6} _{-0.5}	0.0808	105.0 ± 18.0	22	-7.33
J220048.67+123612.4 ^b	sdO	18.6	64200 ± 2600	5.63 ± 0.11	-1.3 ± 0.1	11.4 ^{+1.8} _{-1.6}	2437.2535	53.0 ± 9.5	3	-7.04
J153752.95+160201.8	sdB	18.4	32300 ± 500	5.47 ± 0.07	< -3.0	8.5 ^{+0.9} _{-0.9}	0.0361	68.0 ± 12.5	3	-7.03
J183229.22+402418.4	sdO	15.7	40100 ± 600	5.35 ± 0.11	-2.0 ± 0.2	3.3 ^{+0.3} _{-0.4}	3.0098	50.0 ± 11.5	5	-6.82
J181126.83+233413.7	sdB	18.4	—	—	—	—	1.0156	121.0 ± 20.5	7	-6.47
J204448.63+153638.8 ^a	sdB	17.9	29600 ± 600	5.57 ± 0.09	-2.2 ± 0.1	5.7 ^{+0.7} _{-0.7}	3.0489	101.0 ± 17.5	7	-6.41
J185414.11+175200.2	sdOB	16.9	35200 ± 700	5.89 ± 0.08	-1.4 ± 0.1	2.9 ^{+0.3} _{-0.3}	6.0874	81.0 ± 22.0	10	-6.25
J171629.92+575121.2 ^a	sdOB	18.2	37500 ± 800	5.57 ± 0.10	< -0.7	7.8 ^{+1.0} _{-0.9}	3195.9096	67.0 ± 15.5	12	-6.14
J184434.74+412158.7	sdB	17.3	27200 ± 500	5.57 ± 0.12	-2.6 ± 0.1	4.0 ^{+0.7} _{-0.6}	2.9795	56.0 ± 14.0	5	-5.72
J091136.73+124015.2	sdB	18.2	—	—	—	—	0.0173	75.0 ± 16.5	3	-5.31
J151337.80+195012.5	sdB	18.9	—	—	—	—	0.0354	98.0 ± 33.5	4	-5.16
J172727.55+091215.5 ⁱ	sdO	17.5	40100 ± 1100	5.36 ± 0.09	< -2.1	7.4 ^{+0.9} _{-0.8}	0.0141	55.0 ± 10.5	6	-5.10
J112242.69+613758.5 ^a	sdB	15.4	29300 ± 500	5.69 ± 0.10	-2.3 ± 0.3	1.5 ^{+0.2} _{-0.2}	0.0469	83.0 ± 18.5	6	-5.08
J161140.50+201857.0 ^a	sdOB	18.5	36900 ± 700	5.89 ± 0.13	-1.2 ± 0.1	6.1 ^{+1.1} _{-0.9}	0.9472	108.0 ± 23.5	5	-4.77
J065044.30+383133.7	sdOB	17.3	34200 ± 400	5.76 ± 0.07	-2.9 ± 0.2	3.9 ^{+0.4} _{-0.3}	0.0131	88.0 ± 13.5	14	-4.63
J170645.57+243208.6 ^a	sdB	17.8	32000 ± 500	5.59 ± 0.07	< -4.0	5.5 ^{+0.6} _{-0.6}	0.0125	46.0 ± 12.0	3	-4.41
J083359.65-043521.9	sdOB	18.3	36100 ± 500	5.92 ± 0.11	-1.9 ± 0.2	5.5 ^{+0.8} _{-0.7}	14.9765	88.0 ± 25.5	11	-4.39
J140545.25+014419.0 ^a	sdB	15.8	27300 ± 800	5.37 ± 0.16	-1.9 ± 0.2	2.5 ^{+0.6} _{-0.5}	0.0263	25.0 ± 8.0	3	-4.12
J160534.96+062733.5	sdB	19.3	—	—	—	—	1.0113	132.0 ± 41.0	8	-3.97
J221920.67+394603.5	sdO	17.3	47000 ± 3500	5.73 ± 0.16	< -3.0	4.7 ^{+1.2} _{-0.9}	62.8679	66.0 ± 12.5	8	-3.93
J183840.52+400226.8	sdB	17.8	29300 ± 900	5.52 ± 0.13	-1.6 ± 0.2	5.5 ^{+1.1} _{-0.9}	2.9795	74.0 ± 20.0	5	-3.89
J115716.37+612410.7 ^a	sdB	17.2	29900 ± 500	5.59 ± 0.08	-3.2 ± 0.8	4.0 ^{+0.5} _{-0.4}	2250.6902	102.0 ± 27.0	7	-3.63
J113303.70+290223.0 ^a	sdB/DA	18.9	—	—	—	—	0.0158	95.0 ± 30.0	3	-3.39
J161817.65+120159.6 ^a	sdB	18.0	32100 ± 1000	5.35 ± 0.23	< 0.0	8.1 ^{+2.8} _{-2.1}	0.0427	105.0 ± 28.0	4	-3.35
J205101.72+011259.7	sdB+X	17.6	—	—	—	—	0.0141	91.0 ± 31.5	8	-3.28
J133638.81+111949.4 ^a	sdB	17.3	27500 ± 500	5.49 ± 0.08	-2.7 ± 0.2	4.4 ^{+0.5} _{-0.5}	0.0301	48.0 ± 14.0	3	-3.25
J094044.07+004759.6 ^b	sdB	19.1	37000 ± 800	5.82 ± 0.13	-0.1 ± 0.1	8.8 ^{+1.3} _{-1.3}	2982.7971	30.0 ± 8.5	2	-3.24
J210454.89+110645.5 ^a	sdOB	17.3	37800 ± 700	5.63 ± 0.10	-2.4 ± 0.2	4.9 ^{+0.6} _{-0.6}	2548.0064	139.0 ± 27.5	9	-3.14
J211651.96+003328.5 ^a	sdB	18.0	27900 ± 800	5.78 ± 0.15	-3.9 ± 0.7	4.3 ^{+0.9} _{-0.8}	0.0161	47.0 ± 15.0	3	-3.08
J091428.87+125023.8	sdB	18.0	33600 ± 600	5.54 ± 0.11	< -3.0	7.0 ^{+1.1} _{-0.9}	0.0176	49.0 ± 13.5	3	-3.07
J112014.86+412127.3	sdB	18.1	—	—	—	—	1503.8023	23.0 ± 7.5	2	-2.98
J173614.19+335249.5	sdB	18.8	—	—	—	—	0.0410	85.0 ± 26.0	5	-2.97
J092520.70+470330.6 ^a	sdB	17.7	28100 ± 900	5.17 ± 0.15	-2.5 ± 0.2	7.5 ^{+1.7} _{-1.4}	0.0126	40.0 ± 12.5	3	-2.88
J171617.33+553446.7 ^a	sdB	17.2	32900 ± 900	5.48 ± 0.09	< -3.0	4.9 ^{+0.7} _{-0.6}	0.0125	130.0 ± 40.5	9	-2.85
J064809.54+380850.1	sdB	18.4	29300 ± 800	5.26 ± 0.13	-2.8 ± 0.3	9.8 ^{+1.9} _{-1.6}	0.9989	48.0 ± 13.0	5	-2.85
J075937.15+541022.2 ^a	sdB	17.8	31300 ± 700	5.30 ± 0.10	-3.3 ± 0.3	7.6 ^{+1.1} _{-1.0}	0.0233	40.0 ± 18.5	3	-2.75
J001844.33-093855.0	sdB	18.8	—	—	—	—	1169.8455	27.0 ± 8.0	3	-2.75
J130439.57+312904.8 ^a	sdOB	17.1	38100 ± 600	5.69 ± 0.12	-0.4 ± 0.1	4.1 ^{+0.6} _{-0.6}	0.0163	49.0 ± 27.5	3	-2.63
J143347.59+075416.9	sdOB	16.7	36600 ± 600	6.16 ± 0.13	< -0.5	1.9 ^{+0.3} _{-0.3}	805.7659	52.0 ± 10.5	11	-2.61
J153540.30+173458.8	sdB	18.0	—	—	—	—	0.0168	58.0 ± 16.5	3	-2.57
J202758.63+773924.5 ^a	sdO	17.9	46200 ± 3200	5.48 ± 0.18	-2.8 ± 0.9	8.2 ^{+2.2} _{-1.8}	1.9601	114.0 ± 33.0	3	-2.48
J215648.71+003620.7 ^a	sdB	18.0	30800 ± 800	5.77 ± 0.12	-2.2 ± 0.3	4.7 ^{+0.8} _{-0.7}	822.1114	100.0 ± 28.0	6	-2.38
J073701.45+225637.6	sdB	16.8	28100 ± 300	5.45 ± 0.04	< -3.0	3.7 ^{+0.2} _{-0.2}	2.0639	53.0 ± 14.5	5	-2.36
J220810.05+115913.9	sdB	17.4	27200 ± 600	5.23 ± 0.07	-2.3 ± 0.3	6.1 ^{+0.6} _{-0.6}	2172.7020	42.0 ± 12.5	5	-2.31
J172919.04+072204.5	sdO	17.3	49200 ± 1900	5.78 ± 0.12	-3.0 ± 0.4	4.6 ^{+0.8} _{-0.7}	0.0179	58.0 ± 20.0	5	-2.22
J031226.01+001018.2	sdB	19.2	—	—	—	—	2552.8670	71.0 ± 30.5	2	-2.17
J204546.81-054355.6 ^a	sdB	17.9	35500 ± 500	5.47 ± 0.09	-1.4 ± 0.2	7.3 ^{+0.9} _{-0.8}	0.0128	41.0 ± 16.5	4	-2.15
J133200.95+673325.7	sdOB	17.2	37400 ± 500	5.90 ± 0.09	-1.5 ± 0.1	3.4 ^{+0.4} _{-0.4}	2584.9083	53.0 ± 14.5	7	-2.09
J120427.94+172745.3	sdB	18.3	25100 ± 900	5.25 ± 0.15	-2.6 ± 0.4	8.2 ^{+1.9} _{-1.9}	0.0282	68.0 ± 29.0	3	-2.05
J204550.97+153536.3	sdB	18.2	30300 ± 500	5.62 ± 0.09	< -3.0	6.3 ^{+0.8} _{-0.7}	5.9148	58.0 ± 13.5	7	-1.98
J135807.96+261215.5 ^a	sdB	17.9	33500 ± 600	5.66 ± 0.10	> +2.0	5.8 ^{+0.8} _{-0.7}	0.0302	86.0 ± 26.0	6	-1.89
J113935.45+614953.9 ^a	sdB	16.9	28800 ± 900	5.27 ± 0.15	-2.8 ± 0.3	4.9 ^{+1.1} _{-0.9}	0.0112	30.0 ± 10.5	3	-1.86
J155343.39+131330.4	sdOB	18.5	36300 ± 500	5.63 ± 0.16	-0.8 ± 0.1	8.1 ^{+1.7} _{-1.4}	0.0160	64.0 ± 24.0	3	-1.77

Name	Class	m_V [mag]	T_{eff} [K]	$\log g$	$\log y$	d [kpc]	Δt [d]	ΔRV_{max} [km s ⁻¹]	N	$\log p$
J082657.29+122818.1	sdOB	17.1	36500 ± 400	5.83 ± 0.12	-1.4 ± 0.1	3.4 ^{+0.5} _{-0.5}	0.0142	67.0 ± 22.0	4	-1.73
J152705.03+110843.9 ^a	sdOB	17.3	37600 ± 500	5.62 ± 0.10	-0.5 ± 0.1	4.8 ^{+0.6} _{-0.5}	0.0543	43.0 ± 12.0	5	-1.73
J052544.93+630726.0 ^a	sdOB	17.7	35600 ± 800	5.85 ± 0.10	-1.6 ± 0.2	4.3 ^{+0.6} _{-0.5}	0.0264	42.0 ± 15.0	5	-1.73
J100535.76+223952.1 ^a	sdB	18.4	29000 ± 700	5.43 ± 0.13	-2.7 ± 0.2	7.9 ^{+1.5} _{-1.7}	0.0192	41.0 ± 14.0	4	-1.71
J164204.37+440303.2	sdB	16.8	29300 ± 800	5.09 ± 0.13	-2.5 ± 0.3	5.7 ^{+1.1} _{-0.9}	0.0273	31.0 ± 11.5	4	-1.68
J090957.82+622927.0	sdO	16.4	48000 ± 4900	5.68 ± 0.17	-1.7 ± 0.6	3.4 ^{+1.0} _{-0.8}	0.0461	37.0 ± 12.0	4	-1.64
J152458.81+181940.5	sdO	18.3	52300 ± 2500	5.28 ± 0.08	-2.8 ± 0.3	13.5 ^{+1.7} _{-1.5}	0.0155	41.0 ± 15.0	3	-1.60
J112140.20+183613.7	sdB	18.6	28100 ± 500	5.46 ± 0.10	-1.8 ± 0.1	8.3 ^{+1.0} _{-1.0}	0.9796	71.0 ± 26.0	4	-1.57
J151254.55+150447.0	sdOB	17.8	38300 ± 600	6.01 ± 0.10	-1.5 ± 0.2	4.0 ^{+0.5} _{-0.5}	0.0229	65.0 ± 28.0	3	-1.54
J233406.11+462249.3 ^a	sdB	17.7	34600 ± 500	5.71 ± 0.09	-1.3 ± 0.1	4.9 ^{+0.6} _{-0.6}	0.0248	31.0 ± 12.0	3	-1.53
J095054.97+460405.2	sdB	18.0	28500 ± 500	5.24 ± 0.07	-2.3 ± 0.3	8.1 ^{+0.8} _{-0.8}	0.0390	42.0 ± 16.5	3	-1.52
J112526.95+112902.6	sdOB	17.4	36100 ± 700	6.06 ± 0.12	-0.8 ± 0.1	2.9 ^{+0.8} _{-0.4}	0.0142	70.0 ± 31.0	4	-1.50
J163834.68+265110.2	sdOB	17.0	36000 ± 300	5.80 ± 0.05	-1.6 ± 0.1	3.4 ^{+0.2} _{-0.3}	0.0159	40.0 ± 13.0	4	-1.50
J203017.81+131849.2	sdOB	16.8	37100 ± 500	5.92 ± 0.09	-1.4 ± 0.1	2.7 ^{+0.3} _{-0.3}	1200.7860	52.0 ± 20.0	5	-1.47
J130059.20+005711.7 ^a	sdOB	16.5	40700 ± 500	5.53 ± 0.10	-0.6 ± 0.1	3.9 ^{+0.3} _{-0.4}	0.0123	36.0 ± 14.5	3	-1.43

Notes. ^(a) Atmospheric parameters taken from Geier et al. (2011a). ^(b) Atmospheric parameters taken from Kupfer et al. (2015). ^(c) Atmospheric parameters taken from Geier et al. (2011b). ^(d) Atmospheric parameters taken from Schaffenroth et al. (2014). ^(e) Atmospheric parameters taken from Østensen et al. (2013). ^(f) Atmospheric parameters taken from Schaffenroth et al. in prep. ^(g) Atmospheric parameters taken from Geier et al. (2011c). ^(h) Atmospheric parameters derived from a spectrum taken with ESO-VLT/FORS1. ⁽ⁱ⁾ Atmospheric parameters derived from a spectrum taken with WHT/ISIS.

Table 4. Parameters of 25 helium-rich hot subdwarfs (14 RV variable, 11 RV variable candidates).

Name	Class	m_V [mag]	T_{eff} [K]	$\log g$	$\log y$	d [kpc]	Δt [d]	ΔRV_{max} [km s ⁻¹]	N	$\log p$
J232757.46+483755.2 ^a	He-sdO	15.8	64700 ± 2000	5.40 ± 0.08	> +2.0	4.2 ^{+0.5} _{-0.4}	1799.6136	176.0 ± 20.5	59	-680.31
J141549.05+111213.9 ^a	He-sdO	16.1	43100 ± 800	5.81 ± 0.17	> +2.0	2.4 ^{+0.3} _{-0.4}	0.0075	125.0 ± 17.0	35	-86.42
J103549.68+092551.9 ^a	He-sdO	16.3	48100 ± 600	6.02 ± 0.13	> +2.0	2.2 ^{+0.4} _{-0.3}	3541.9636	53.0 ± 4.0	6	-54.25
J170045.09+391830.3	He-sdOB	18.2	36500 ± 1600	5.87 ± 0.16	+0.1 ± 0.1	5.5 ^{+1.2} _{-1.0}	2160.0414	118.0 ± 11.5	10	-44.76
J161014.87+045046.6	He-sdO	17.3	48400 ± 1400	6.31 ± 0.09	> +2.0	2.5 ^{+0.3} _{-0.2}	0.0124	138.0 ± 17.0	14	-31.77
J110215.45+024034.1 ^a	He-sdO	17.5	56600 ± 4200	5.36 ± 0.22	> +2.0	8.9 ^{+3.0} _{-2.2}	0.0332	62.0 ± 8.5	3	-10.91
J174516.32+244348.3 ^a	He-sdO	17.7	43400 ± 1000	5.62 ± 0.21	> +2.0	6.2 ^{+1.8} _{-1.4}	1220.5806	134.0 ± 25.5	13	-8.81
J160304.07+165953.8 ^b	He-sdO	16.9	45400 ± 300	6.10 ± 0.07	> +2.0	2.5 ^{+0.2} _{-0.2}	0.9087	71.0 ± 18.5	5	-8.11
J094856.95+334151.0 ^a	He-sdO	17.7	51000 ± 1200	5.87 ± 0.12	+1.8 ± 0.5	5.1 ^{+0.8} _{-0.7}	0.0123	74.0 ± 14.0	3	-7.73
J152136.25+162150.3	He-sdO	17.1	47400 ± 1000	5.81 ± 0.08	+1.6 ± 0.4	4.0 ^{+0.4} _{-0.4}	2175.9687	77.0 ± 24.0	9	-5.94
J163416.08+221141.0	He-sdOB	15.5	38300 ± 1400	5.65 ± 0.26	> +2.0	2.0 ^{+0.8} _{-0.6}	653.3309	35.0 ± 6.5	6	-5.55
J153237.94+275636.9	He-sdO	18.5	37700 ± 1300	6.09 ± 0.22	+0.0 ± 0.2	5.0 ^{+1.5} _{-1.2}	1.0012	73.0 ± 16.5	3	-5.52
J233914.00+134214.3	He-sdO	17.6	48100 ± 1600	5.65 ± 0.25	> +2.0	6.0 ^{+2.1} _{-1.6}	1451.6391	72.0 ± 11.8	12	-5.11
J173034.09+272139.8 ^c	He-sdO	18.9	39500 ± 700	5.83 ± 0.17	+0.1 ± 0.1	8.1 ^{+1.8} _{-1.5}	698.7112	41.0 ± 10.0	2	-5.00
J170214.00+194255.1 ^b	He-sdO	15.8	44300 ± 600	5.79 ± 0.11	> +2.0	2.1 ^{+0.3} _{-0.3}	1665.2088	38.0 ± 10.0	5	-3.76
J081329.81+383326.9	He-sdO	17.5	45800 ± 800	6.11 ± 0.11	+1.8 ± 0.4	3.3 ^{+0.3} _{-0.4}	0.0175	54.0 ± 13.0	6	-3.35
J204940.85+165003.6 ^a	He-sdO	17.9	43000 ± 700	5.71 ± 0.13	> +2.0	6.2 ^{+1.1} _{-0.9}	5.9325	84.0 ± 18.5	7	-3.13
J160623.21+363005.4	He-sdOB	18.5	36400 ± 700	5.34 ± 0.17	-0.5 ± 0.1	11.3 ^{+2.6} _{-2.1}	1414.9811	67.0 ± 19.5	2	-3.04
J112414.45+402637.1 ^a	He-sdO	18.0	47100 ± 1000	5.81 ± 0.23	> +1.7	5.9 ^{+1.9} _{-1.4}	0.0215	62.0 ± 18.5	3	-2.65
J161059.80+053625.2 ^b	He-sdO	17.2	46300 ± 700	6.22 ± 0.10	+1.0 ± 0.6	2.6 ^{+0.3} _{-0.3}	751.7674	38.0 ± 9.5	4	-2.64
J151415.66-012925.2 ^a	He-sdO	17.0	48200 ± 500	5.85 ± 0.08	+1.7 ± 0.4	3.6 ^{+0.4} _{-0.3}	3.9687	66.0 ± 20.5	5	-2.58
J161938.64+252122.4	He-sdOB	17.5	35000 ± 2000	5.80 ± 0.33	-0.4 ± 0.2	4.3 ^{+2.1} _{-1.5}	0.9716	67.0 ± 26.0	3	-1.81
J160450.44+051909.2	He-sdOB	18.5	38100 ± 700	5.22 ± 0.27	+1.2 ± 0.2	13.7 ^{+3.2} _{-3.8}	0.9736	145.0 ± 61.0	8	-1.75
J090252.99+073533.9	He-sdO	17.4	40100 ± 500	5.91 ± 0.19	> +2.0	3.7 ^{+0.9} _{-0.7}	1612.4334	67.0 ± 27.0	5	-1.65
J081304.04-071306.5	He-sdO	18.6	48200 ± 900	5.93 ± 0.14	+1.8 ± 0.5	7.0 ^{+1.3} _{-1.1}	0.9897	137.0 ± 41.0	7	-1.50

Notes. ^(a) Atmospheric parameters taken from Geier et al. (2011a). ^(b) Atmospheric parameters derived from a spectrum taken with ESO-VLT/FORS1. ^(c) Atmospheric parameters derived from a spectrum taken with WHT/ISIS.

Table 5. Parameters of 13 other types of hot stars (7 RV variable, 6 RV variable candidates).

Name	Class	m_V [mag]	T_{eff} [K]	$\log g$	$\log y$	d [kpc]	Δt [d]	ΔRV_{max} [km s ⁻¹]	N	$\log p$
J131916.15-011404.9	BHB	16.4	17400 ± 800	4.55 ± 0.15	-1.9 ± 0.2	5.9 ^{+1.4} _{-1.1}	2888.0925	46.0 ± 9.0	8	-42.10
J164121.22+363542.7	BHB	17.4	19300 ± 1000	4.55 ± 0.10	-1.9 ± 0.2	9.9 ^{+1.7} _{-1.4}	1035.9093	99.0 ± 9.0	8	-39.13
J075732.18+184329.3 ^a	O(He)	18.6	80000 ± 2000	5.00 ± 0.30	> +2.0	29.6 ^{+12.7} _{-9.0}	0.0216	107.0 ± 22.0	6	-30.13
J155610.40+254640.3 ^b	PG 1159	17.9	100000 ⁺¹⁵⁰⁰⁰ ₋₁₀₀₀₀	5.3 ± 0.3	> +2.0	16.9 ^{+8.9} _{-5.9}	231.1694	116.0 ± 21.0	10	-17.98
J201302.58-105826.1	MS-B	18.5	16400 ± 1400	4.30 ± 0.27	-1.3 ± 0.2	51.8 ^{+25.6} _{-16.4}	2.0155	61.0 ± 11.5	8	-13.42
J093521.39+482432.4	O(H)	18.5	87700 ± 20000	5.68 ± 0.16	-1.0 ± 0.3	12.0 ^{+3.7} _{-3.3}	2269.7542	38.0 ± 7.5	2	-6.97
J161253.21+060538.7	MS-B	15.5	15700 ± 1400	4.18 ± 0.29	-1.0 ± 0.2	14.4 ^{+7.2} _{-4.8}	811.5968	38.0 ± 7.0	10	-6.84
J020531.40+134739.8 ^c	BHB	18.4	17400 ± 700	4.26 ± 0.13	-1.7 ± 0.2	20.3 ^{+4.0} _{-3.4}	2781.1087	28.0 ± 7.0	3	-3.64
J144023.58+135454.7	BHB	18.3	18900 ± 700	4.50 ± 0.15	-1.9 ± 0.3	16.1 ^{+3.6} _{-3.0}	0.0528	78.0 ± 24.0	4	-3.15
J171947.87+591604.2	MS-B	16.9	15100 ± 600	4.10 ± 0.19	-0.9 ± 0.2	29.2 ^{+8.3} _{-6.5}	2568.7218	32.0 ± 6.5	10	-3.11
J100019.98-003413.3	O(H)	17.8	93700 ± 10700	5.88 ± 0.10	-0.6 ± 0.2	7.3 ^{+1.3} _{-1.1}	3.0114	135.0 ± 28.0	16	-2.20
J110256.32+010012.3 ^c	BHB	18.5	17300 ± 800	4.32 ± 0.14	-2.1 ± 0.2	19.5 ^{+4.3} _{-3.5}	2735.5338	24.0 ± 9.0	3	-1.77
J204149.38+003555.8 ^c	BHB	19.0	19400 ± 2200	4.02 ± 0.29	-2.1 ± 0.4	38.3 ^{+20.3} _{-13.4}	38.0700	26.0 ± 10.5	3	-1.71

Notes. ^(a) Atmospheric parameters taken from Werner et al. (2014). ^(b) Atmospheric parameters taken from Reindl et al. (2015). ^(c) Atmospheric parameters derived from a spectrum taken with ESO-VLT/FORS1.

Table A.1. Parameters of 19 stars with non-significant RV variations.

Name	Class	m_V [mag]	T_{eff} [K]	$\log g$	$\log y$	d [kpc]	Δt [d]	ΔRV_{max} [km s ⁻¹]	N	$\log p$
J085727.65+424215.4 ^a	He-sdO	18.5	39500 ± 1900	5.63 ± 0.24	+0.2 ± 0.2	8.7 ^{+3.0} _{-2.2}	0.0657	111.0 ± 39.5	4	-1.26
J074551.13+170600.3	sdOB	17.1	35600 ± 400	5.54 ± 0.05	-2.8 ± 0.1	4.7 ^{+0.3} _{-0.3}	9.9390	65.0 ± 12.0	18	-1.26
J110445.01+092530.9 ^a	sdOB	16.3	35900 ± 800	5.41 ± 0.07	-2.1 ± 0.4	3.8 ^{+0.4} _{-0.3}	0.0396	34.0 ± 12.0	4	-1.25
J012739.35+404357.8 ^a	sdO	16.8	48300 ± 3200	5.67 ± 0.10	-1.3 ± 0.2	4.1 ^{+0.7} _{-0.6}	0.0369	45.0 ± 17.0	8	-1.23
J172816.87+074839.0	sdB	18.4	30700 ± 700	5.37 ± 0.09	-2.5 ± 0.4	9.0 ^{+1.2} _{-1.1}	1.9962	75.0 ± 34.0	7	-1.11
J143153.05-002824.3 ^a	sdOB	18.1	37300 ± 800	6.02 ± 0.16	-0.8 ± 0.1	4.4 ^{+0.9} _{-0.8}	0.0120	64.0 ± 20.5	8	-1.05
J225150.80-082612.7 ^b	BHB	18.4	19000 ± 500	4.98 ± 0.09	-1.8 ± 0.3	9.5 ^{+1.3} _{-1.1}	2411.2964	20.0 ± 7.0	5	-1.04
J074806.15+342927.7	sdOB	17.3	35100 ± 800	5.72 ± 0.08	-1.7 ± 0.1	4.3 ^{+0.5} _{-0.5}	5.9453	42.0 ± 12.5	12	-0.95
J111225.70+392332.7	sdOB	17.6	37800 ± 500	5.76 ± 0.11	-0.6 ± 0.1	4.9 ^{+0.7} _{-0.6}	0.0563	104.0 ± 28.0	13	-0.92
J134352.14+394008.3 ^a	He-sdOB	18.2	36000 ± 2100	4.78 ± 0.30	-0.2 ± 0.2	18.8 ^{+8.5} _{-6.1}	0.0224	53.0 ± 27.0	3	-0.89
J163702.78-011351.7 ^a	He-sdO	17.3	46100 ± 700	5.92 ± 0.22	> +2.0	3.8 ^{+1.1} _{-0.9}	0.0853	100.0 ± 42.5	12	-0.85
J174442.35+263829.9	sdOB	17.9	–	–	–	–	0.0384	88.0 ± 44.0	7	-0.84
J180757.08+230133.0	He-sdO	17.1	42700 ± 1000	6.04 ± 0.21	> +2.0	2.9 ^{+0.8} _{-0.7}	0.9992	39.0 ± 19.0	4	-0.83
J204623.12-065926.8	O(H)	17.7	79500 ± 12500	5.74 ± 0.13	-1.1 ± 0.2	7.6 ^{+1.6} _{-1.6}	1376.1081	47.0 ± 18.0	5	-0.64
J075818.49+102742.5	sdOB	16.4	37400 ± 600	5.51 ± 0.05	< -3.0	3.6 ^{+0.2} _{-0.2}	0.0596	32.0 ± 12.5	6	-0.57
J215053.84+131650.5	sdB+X	17.0	–	–	–	–	0.0154	24.0 ± 13.5	4	-0.56
J215307.34-071948.3	sdB	17.1	33100 ± 1300	5.74 ± 0.15	-2.0 ± 0.2	3.6 ^{+0.8} _{-0.7}	24.9831	50.0 ± 27.5	13	-0.42
J113418.00+015322.1 ^a	sdB	17.7	29700 ± 1200	4.83 ± 0.16	< -4.0	11.8 ^{+2.9} _{-2.4}	0.0757	46.0 ± 20.0	6	-0.42
J170716.53+275410.4	sdB	16.7	30200 ± 1400	5.62 ± 0.16	< -3.0	3.1 ^{+0.8} _{-0.6}	0.0124	52.0 ± 23.0	9	-0.21

Notes. ^(a) Atmospheric parameters taken from Geier et al. (2011a). ^(b) Atmospheric parameters derived from a spectrum taken with ESO-VLT/FORS1.